Acceleration and demographic rates behind bird decline in North America

François Leroy [1,], Marta A. Jarzyna [2,3], Petr Keil [1]*

[1]Department of Spatial Sciences, Faculty of Environmental Sciences, Czech University of Life Sciences Prague, Kamýcká 129, 16500 Praha-Suchdol, Czech Republic

[2] Department of Evolution, Ecology and Organismal Biology, The Ohio State University, Columbus, Ohio, 43210, USA

[3] Translational Data Analytics Institute, The Ohio State University, Columbus, Ohio, 43210, USA

Acceleration of human activities over the past century might have caused a corresponding acceleration in the decline of abundance of species, but this has not been empirically assessed. Further, the temporal dynamics of abundance arises from a complex interaction between recruitment and loss of individuals, which remains unexplored across large spatial scales. We address these gaps by examining temporal changes, acceleration, deceleration, and vital processes (*i.e.* recruitment and loss) across much of the North American avifauna from 1987 to 2021. We confirm the continent-wide decline of bird abundance, and pinpoint the regional hotspots of acceleration of this decline in the Mid-Atlantic region, Midwest, and California, matching broad spatial patterns of human activities. We further reveal that the increasing rate of loss is the primary process responsible for the acceleration of abundance decline in California and the Midwest, whereas a decrease in recruitment rate dominates in the Mid-Atlantic. Finally, we highlight a worrisome trend: 96% of bird species and 100% of families with increasing abundances are concurrently experiencing a decline in recruitment rate. Thus, we need conservation policies even for species that appear to be thriving. Further, simply preventing loss may not be enough, as we also need policies that enhance recruitment.

Over the Anthropocene, human activities have profoundly impacted ecosystems (IPBES, 2019), and a closely monitored indicator of this impact is temporal change in local population abundances. Global reports show an overall decline of abundances, with an average per-species abundance decline estimated to be between 20% (IPBES, 2019) and 69% (Living Planet Index, LPI; < www.livingplanetindex.org/>, but see Leung et al., 2020 for criticism of the LPI). Analyses of local time series show a more complex picture, with some reporting both abundance declines and increases (Daskalova et al., 2020; Dornelas et al., 2023; Inger et al., 2015; Johnson et al., 2024; Leung et al., 2017; Pilotto et al., 2020; Van Klink et al., 2020). A particularly large number of local times series of abundances are available for birds across North America and Europe, revealing an overall decline (Rigal et al., 2023; Rosenberg et al., 2019).

The declines of population abundances have been mainly attributed to human activities (Díaz et al., 2019) such as agricultural intensification (Rigal et al., 2023), changes in land-use, overexploitation, and pollution (Convention on Biological Diversity, 2010; < https://www.cbd.int/convention >). The past century, however, has seen not only the increase but also an *acceleration* of the increase of human activities (Meadows et al., 2017; Piketty, 2014), often termed the Great Acceleration (Hooks, 2019; Steffen et al., 2015), and an acceleration of species loss (Barnosky et al., 2011; Ceballos et al., 2015; Urban, 2015). We should thus expect a corresponding acceleration in population declines, but a

comprehensive analysis of rates of local population changes across large spatial extents and multiple species is lacking. In essence, while the first order derivative of population abundance change for the majority of species appears to be a decline, the second order derivative (*i.e.* acceleration or deceleration of this change) remains unexplored.

While examining the temporal changes in population abundance is valuable, there are ecologically informative demographic processes that govern the dynamics. Abundance change in time, ΔN, arises from the difference between recruitment R (*i.e.* number of new individuals entering the population through birth, maturation, or immigration) and loss L (*i.e.* number of individuals removed from the population by death or emigration, Fig. 1a). To facilitate comparisons among populations of varying sizes, the temporal dynamics can be expressed using vital rates, which are per-capita (a.k.a. per-individual) changes. The growth rate g (*i.e.* the per-capita average change over time) results from the difference between recruitment rate r and loss rate l, representing the per-capita probability of a new individual entering a population or disappearing, respectively (Fig. 1a). The interplay between r, l and how they change with time in real-world population dynamics remains unknown for most species, particularly at large spatiotemporal scales. Bridging this knowledge gap would provide deeper insights into the mechanisms of the ongoing biodiversity crisis and help shape effective conservation strategies.

Here, we provide a comprehensive assessment of temporal changes in local population abundances of 508 bird species across North America from 1987 to 2021, focusing on acceleration, deceleration, recruitment, and loss. Using 1,033 routes of the North American Breeding Bird Survey (Ziolkowski Jr. et al., 2022) (BBS) and advances in N-mixture population models (Dail & Madsen, 2011; Kéry & Royle, 2020), we demonstrate widespread bird population declines across North America, pinpoint regions where population declines accelerate or decelerate, and unveil their demographic components. We identify regional acceleration hotspots in the Midwest and California, primarily driven by the increasing loss of individuals, and in the Mid-Atlantic, where decreasing recruitment emerges as the main process. Finally, we unveil an alarming trend in which 96% of species and 100% of avian families with increasing abundances are simultaneously undergoing a decline in recruitment rate, underscoring a hidden vulnerability of seemingly thriving species.

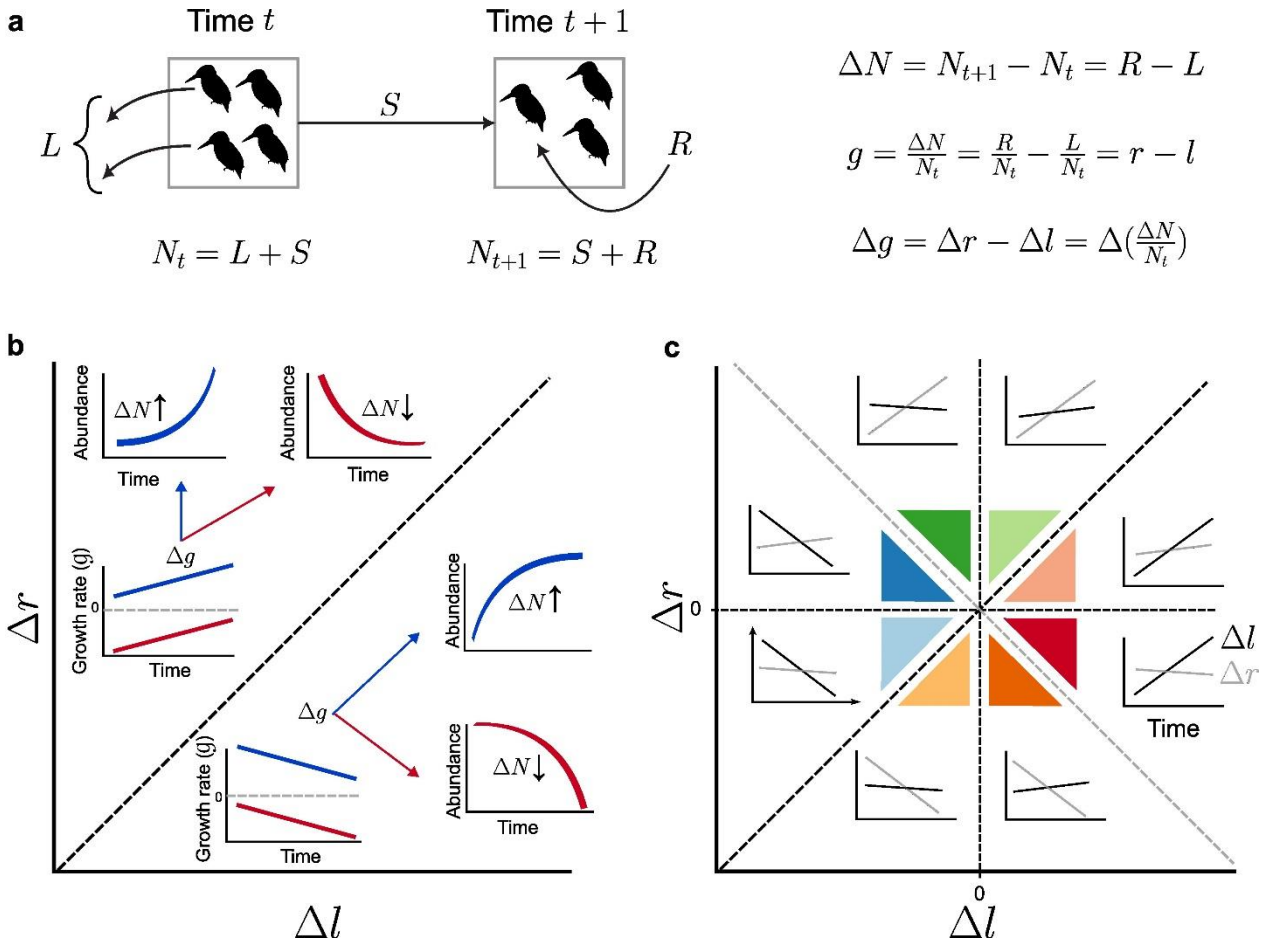

Fig. 1 | Components of temporal change of abundance. a, Relations between individual abundance (N), number of lost individuals (L), recruited individuals (R), survivors (S), and change in abundance (ΔN). They can be expressed as per-capita rates: growth rate (g), recruitment rate (r), loss rate (l), and their respective change (Δg, Δr, Δl). Importantly, Δg is indicative of acceleration or deceleration of ΔN. **b**, Each route, species, family, or habitat type can be mapped onto a $\Delta l \Delta r$ space, indicating a Δg value. Above the black dotted diagonal, growth rate increases (i.e. positive Δg); below, growth rate declines (i.e. negative Δg). Arrows (↑ and ↓) indicate abundance increases (positive ΔN) and declines (negative ΔN); Δg indicate its acceleration or deceleration. **c**, In the same $\Delta l \Delta r$ space, colors indicate the dominant process: blue is dominant negative Δl, green is dominant positive Δr, orange is dominant negative Δr and, red is dominant positive Δl. Inset plots show Δl (black line) and Δr (grey line).

Continental decline in bird populations. When looking at the total abundance of individual birds of all species together, the average yearly abundance change per route (ΔN, eq. 12) is a significant decline of $\Delta N = -34.0$ individuals (Fig. 2a, t-test, $t(1032) = -52.5$, $p < 0.001$, *Confidence Interval* $(CI) = [-35.3; -32.7]$), representing an average loss of 1,190 birds (out of 5,417 in 1987, *i.e.* 22%) per route from 1987 to 2021. Of the routes surveyed, 96% (989) experienced a decline in total bird abundance, and only 44 underwent increases. Using a spatial smoother to show average regional trends not obscured by local variation, we reveal that bird abundances in Florida, Delaware, Texas, and New Jersey underwent the most pronounced average declines (-40.1, -39.8, -39.5 and -39.1 individuals, respectively; Fig. 2b). The change of the per-capita growth rate relative to the size of the initial population in 1987 (Δg_{t1}, eq. 14) was a significant decline (Fig. 2c, $\Delta g_{t1} = -0.0061$ (Fig. 2C, $t(1032) = -59.2$, $p < 0.001$, $CI = [-0.0063; -0.0059]$), which is equivalent to a decline of *ca.* 215 birds per 1000 individuals over 35

years. Vermont, New Jersey, Arizona, and Texas experienced the most pronounced negative Δg_{t1} (-8.72×10^{-3}, -7.68×10^{-3},-7.26×10^{-3}, and -7.25×10^{-3} respectively).

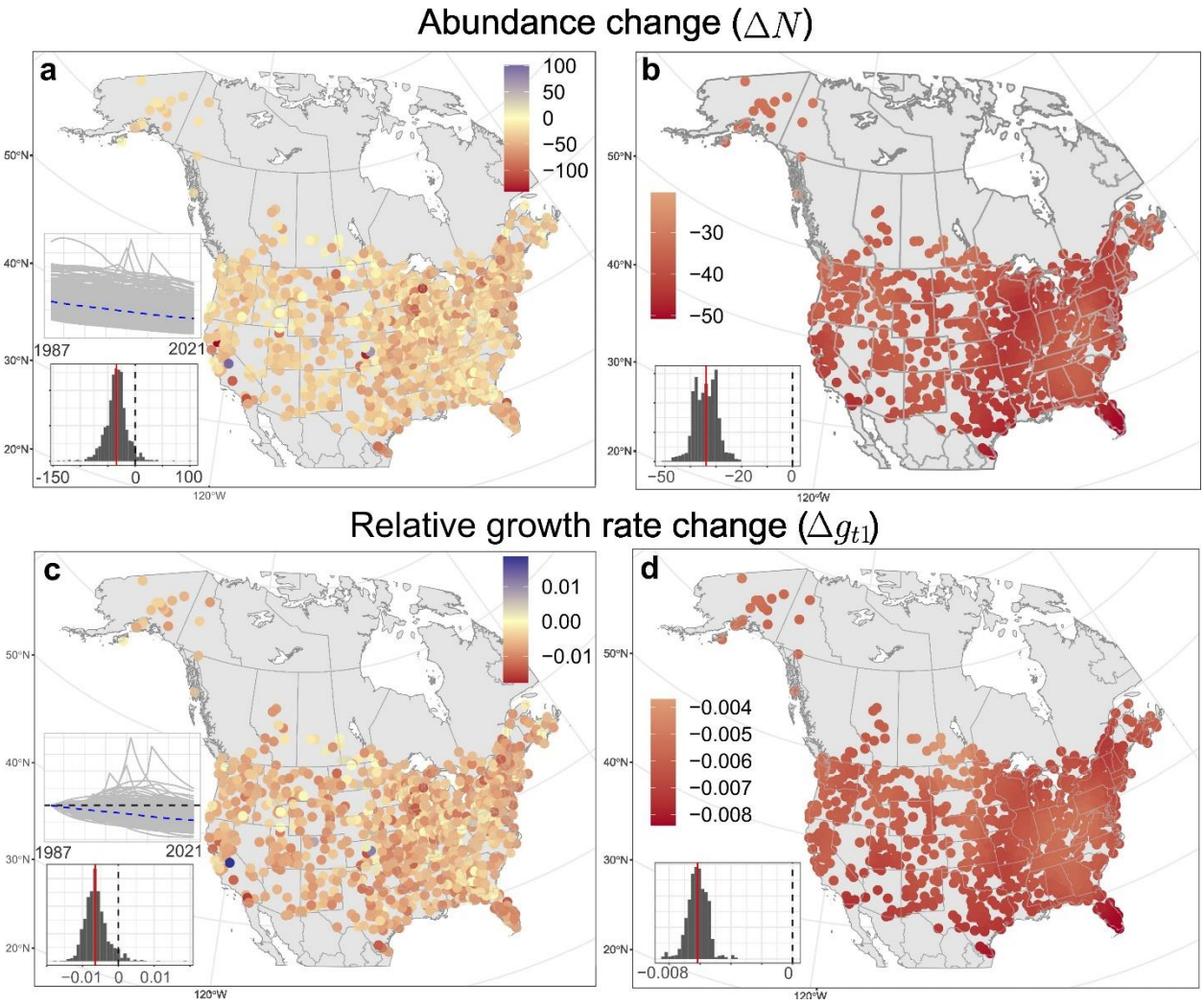

Fig 2 | Temporal change of abundance. a, Abundance change (ΔN) in bird populations from 1987 to 2021. Each dot represents the coefficient of a linear regression between abundance and time for one of the 1,033 routes of the North American Breeding Bird Survey. Inset plots in bottom left show abundance trends for each BBS route in grey, with the average trend in blue dashed line. The inset histograms show the distribution of these trends, with the red vertical line indicating the mean. **c**, Temporal change of the relative growth rate (Δg_{t1}) is the per-capita ΔN relative to the size of the initial population in 1987. **b**, ΔN, and **d**, Δg_{t1}, smoothened using a spatial GAM with a gaussian process smoother.

Acceleration of the decline. As the abundance change is mostly negative across North America ($\Delta N < 0$, Fig. 2b), the yearly growth rate change Δg can be interpreted as acceleration (when Δg is negative) or deceleration (when Δg is positive) of population decline. The yearly growth rate change (Δg, eq. 15) averaged across the whole continent showed no significant deviation from zero (Fig. 3a, $\overline{\Delta g} = 1.62 \times 10^{-5}$, $t(1032) = 1.54$, $p = 0.12$, $CI = [-4.45 \times 10^{-6}; 3.70 \times 10^{-6}]$) with 58% (600) and 42% (433) of routes having positive and negative Δg, respectively. In other words, there was no discernible average per-route trend towards acceleration or deceleration of bird population decline across the entire North America. However, the spatial smoothing uncovered variation of regionally averaged Δg

(Fig. 3b). The Mid-Atlantic region of the US (Delaware, Maryland, and New Jersey), the Midwest (especially Indiana, Ohio, Kentucky, Illinois, Wisconsin, and Michigan), and California had negative Δg, indicative of an acceleration of the abundance decline. Conversely, Yukon, New England (Connecticut, Massachusetts, Maine, New Hampshire), Atlantic Canada (New Brunswick, Prince Edward Island, and Nova Scotia), New Mexico, and South Carolina showed a positive Δg, indicating a deceleration of population decline.

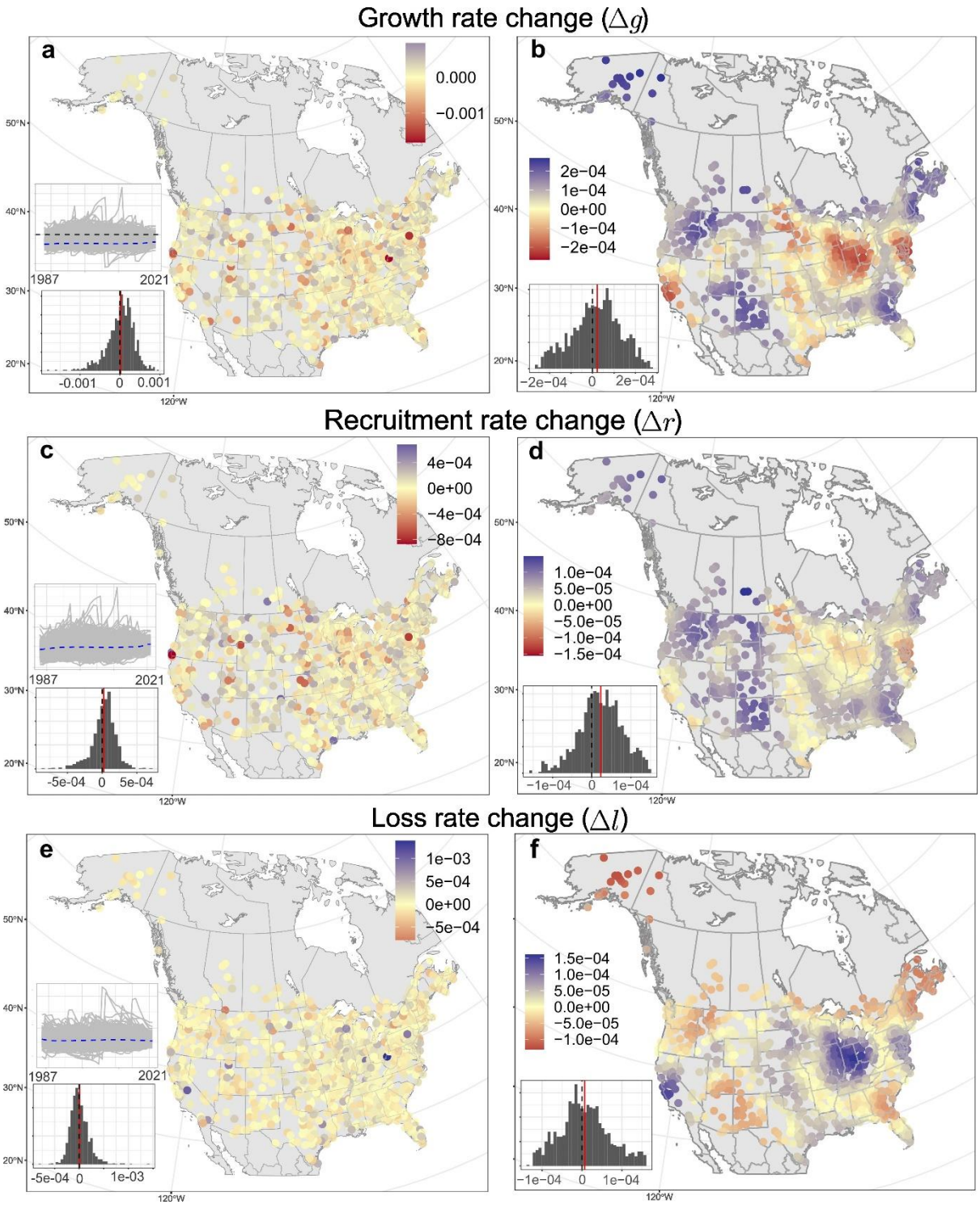

Fig. 3 | Temporal change of per-capita vital rates. a, b, Temporal change of yearly growth rate (Δg) decomposed into (**c,d**) temporal change of recruitment rate (Δr), and (**e,f**) temporal change of loss rate (Δl). Panels on the left (**a,c,e**) show values in each specific Breeding Bird Survey (BBS) route. Panels on the right (**b,d,f**) show regional means obtained from spatial smoothing (using GAM) of the values in the left panels. As abundances are decreasing for all the routes, the smoothened map (**b**) shows regional hotspots of acceleration of bird population decline (in red). Inset plots in bottom left show trends in growth, recruitment, and loss rates for each BBS route in grey, with the average trend in blue dashed line. The histograms show the distribution of these values.

Changes in recruitment and loss rates. At the continental scale, the average temporal change of recruitment rate per route ($\overline{\Delta r}$) was extremely weak but positive at 2.32×10^{-5} (Fig. 3c, $t(1032) = 4.27$, $p = 2.10 \times 10^{-5}$, $CI = [1.25 \times 10^{-5}; 3.38 \times 10^{-5}]$), indicating a yearly increase of 2.32 recruited individuals per 100,000 birds. There were 62% of routes (639) with positive Δr and 38% of routes (394) with negative Δr. The average change in loss rate ($\overline{\Delta l}$) was not significantly different from zero (Fig. 3e, $t(1032) = 1.14$, $p = 0.25$, $\mathrm{CI} = [-5.0 \times 10^{-6}; 1.88 \times 10^{-5}]$), which means that the net per capita loss has not changed at the continental scale since 1987. The smoothened spatial patterns of Δr (Fig. 3c) and Δl (Fig. 3e) match the spatial patterns of Δg (Fig. 3b), with the Mid-Atlantic region (especially Delaware, Maryland, and New Jersey), the Midwest, and California having a combination of negative Δr and positive Δl. In other words, regions that underwent an increase in loss rate also underwent a decrease in recruitment rate.

The main process of the acceleration of population declines: recruitment or loss rate change? Among the 600 routes with positive Δg (*i.e.* decelerating decline), 59% of them had a positive Δr as the primary component (Fig. 4a, green), while negative Δl accounted for 41% of them (Fig. 4a, blue). For the 433 routes with a negative Δg (*i.e.* accelerating decline), 66% showed a positive Δl as the main component (Fig. 4a, red), while it was a negative Δr for 34% of them. Applying the spatial smoother revealed the demographic rates behind the negative Δg (*i.e.* behind the decrease of g in the Midwest, Mid-Atlantic, and California, Fig. 3b): Δl was the main component of the decrease in g across the Midwest and California (Fig. 4d, red), whereas Δr dominated across the Mid-Atlantic (Fig. 4d, orange).

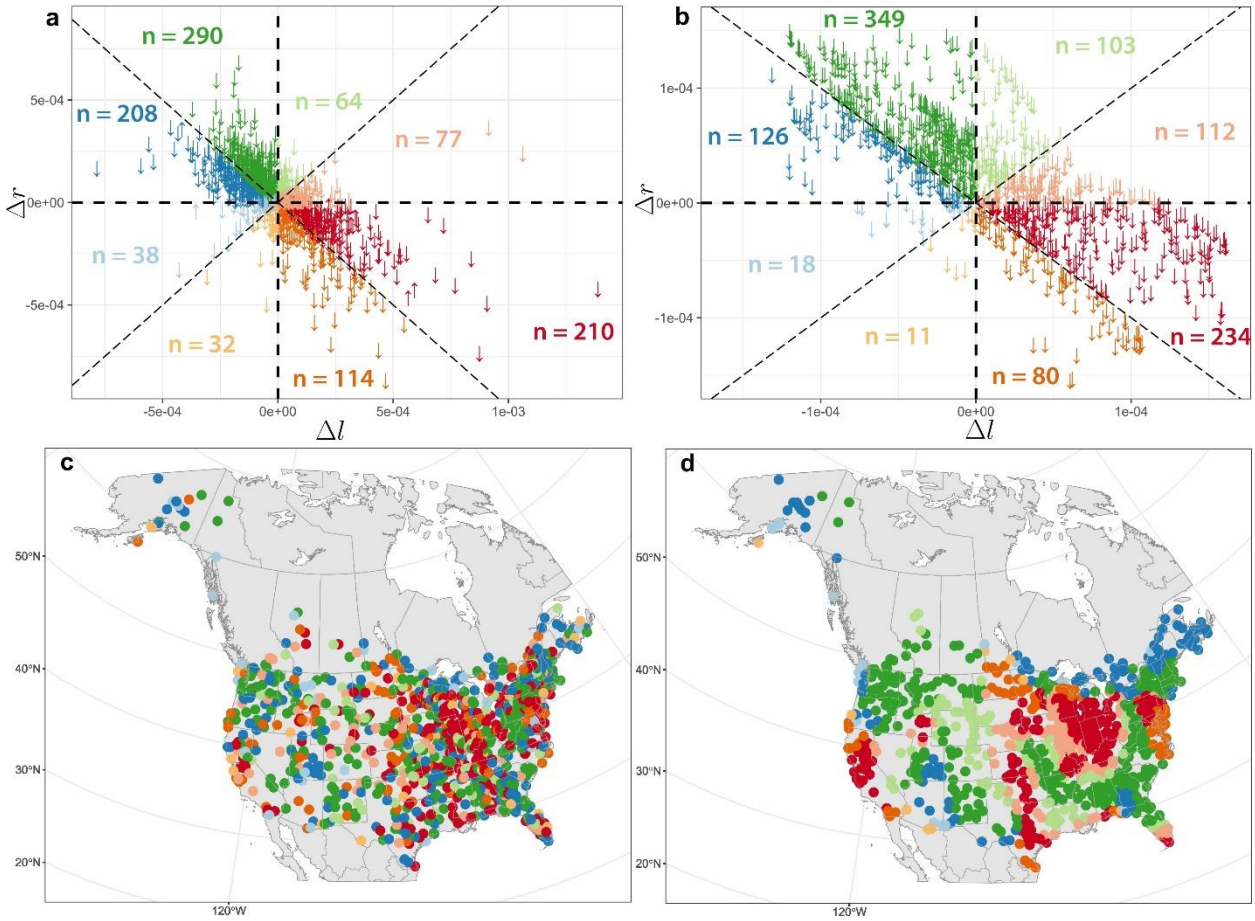

Fig. 4 | Eight classes of temporal change of vital rates. a, Predicted and **b,** spatially smoothened growth rate change (Δg) projected in a loss rate change (Δl) – recruitment rate change (Δr) space. Arrows (↑ and ↓) indicate abundance increases and declines, respectively, for each Breeding Bird Survey route. Colors represent whether the dominant process of Δg is due to negative Δl (blue), positive Δr (green), negative Δr (orange) or positive Δl (red) (see Fig. 1 for details). **c,** and **d,** show spatial distribution of predicted and spatially smoothened values, respectively, with the smoothened map showing the main component of the acceleration in bird population decline.

Per-species, per-family, and per-habitat analyses. We assessed Δg, Δr and Δl at different levels of taxonomic aggregation: species, family, and preferred habitat. Across 508 species, 253 showed positive ΔN of which 98% (247) had negative Δg (Fig. 5a, Fig. 5D, red and orange, Appendix A Fig. 1), particularly with a sharp negative Δr (96%, 237, orange). Additionally, 23 out of 71 families had positive ΔN, of which 100% had negative Δg due to negative Δr (Appendix A Fig. 2). This indicates that nearly all species and families with increasing abundance are experiencing a decrease in growth rate, mainly attributed to a decline in recruitment rate, and are tending toward an eventual decline. At the preferred habitat level, only species associated with the desert showed a positive ΔN (Appendix A Fig. 3) with negative Δg due to a strong negative Δr. Concerning the 255 species with negative ΔN, 63% (161) had negative Δg, while the remaining 37% (94) showed positive Δg. This indicates that nearly two-thirds of the species with declining abundance are undergoing an acceleration of this decline. Species for which the negative Δl was the main process (Fig. 5d, red) represented 45% (114) of the species with negative ΔN.

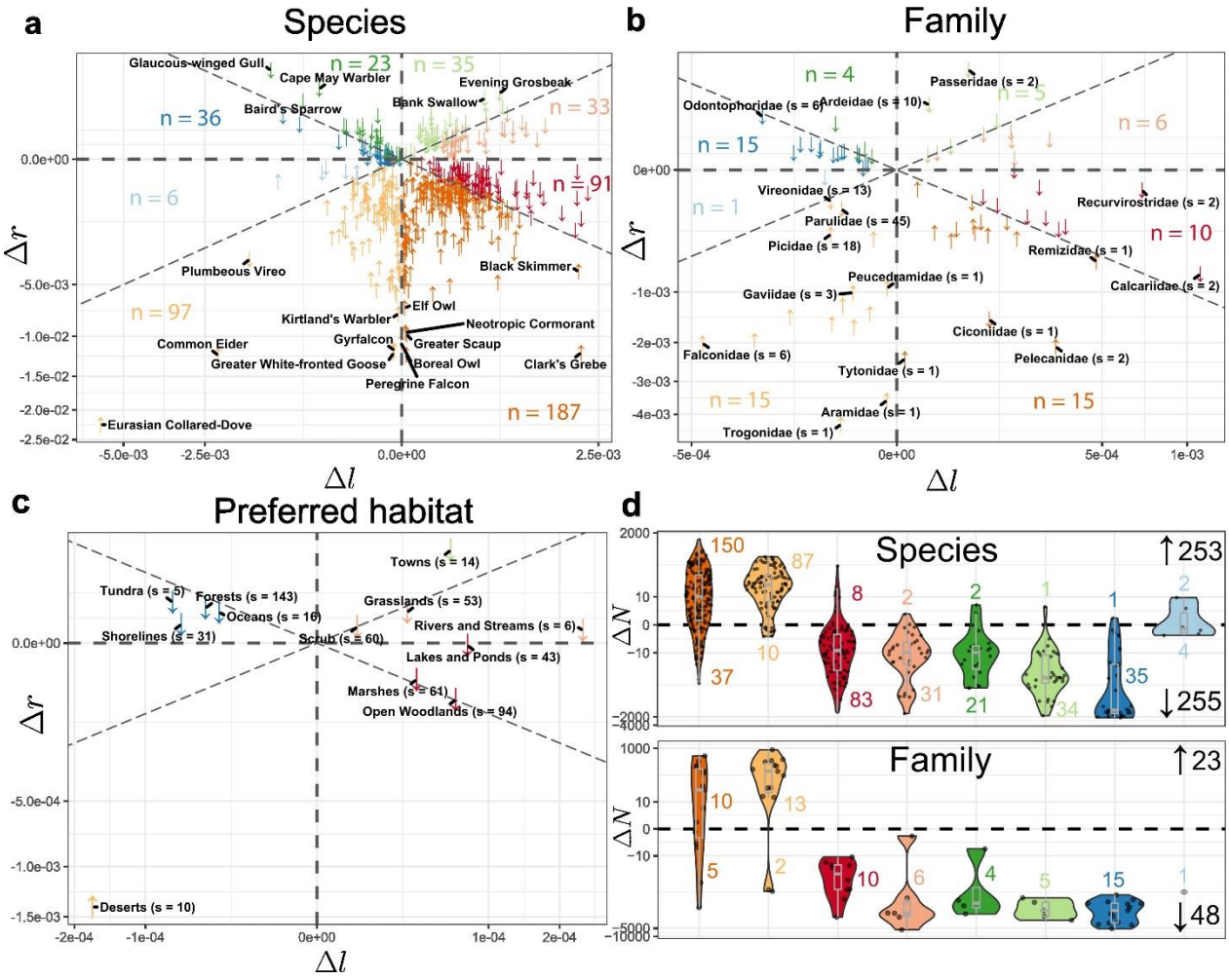

Fig. 5 | Temporal change of vital rates at different levels of taxonomic aggregation. Growth rate change (Δg) projected in a loss rate change (Δl) – recruitment rate change (Δr) space for **a,** all 508 bird species, **b,** 71 avian families, and **c,** 12 preferred habitats. Arrows indicate abundance change (↑ positive and ↓ negative ΔN) for each species, family, and habitat. Species count of each avian family (B) and preferred habitat (C) is designated as s. **d,** Distributions of increasing and decreasing populations ΔN (above and below black dashed line, respectively) falling within each $\Delta l \Delta r$ class for bird species (top panel) and families (bottom panel).

Discussion

Our findings corroborate the decline of bird abundance across North America (Rosenberg et al., 2019) (Fig. 2), and also align with trends seen for some European bird species (Bowler et al., 2019; Fraixedas et al., 2017; Hallmann et al., 2014; Inger et al., 2015; Newton, 2004; Rigal et al., 2023). Here, we go further by identifying specific regions where the decline is accelerating, and we dissect population dynamic into loss and recruitment rates.

Regional hotspots of accelerating bird population decline. We identify the Mid-Atlantic, the Midwest, and California as hotspots of accelerating decline of bird abundance (Fig. 3b). In these regions, the difference between the number of lost and recruited individuals continues to expand every year, raising concerns for the future of these bird populations. The decline of bird abundance has been associated with agricultural intensification (Bowler et al., 2019; Green et al., 2005; Hallmann et al., 2014; Rigal et al.,

2023; Stanton et al., 2018) and changes in land-use (Bowler et al., 2019; Fraixedas et al., 2017). Our findings align with this, as spatial patterns of accelerating decline coincide with those of agriculture (Yan & Roy, 2016), which has intensified in North America (Stanton et al., 2018). The spatial hotspots of accelerating decline also align with patterns of human population density, particularly in the eastern USA and along the West Coast (U. S. Census Bureau, http://www.census.gov). This suggests that regions experiencing an acceleration in human activities are also witnessing an acceleration in bird population decline. Acceleration of human impacts on ecosystems can lead to population collapse, as already observed for both terrestrial (Newbold et al., 2020; Reid et al., 2021) and marine ecosystems (Chen et al., 2016; Frank et al., 2005; Jackson et al., 2001). This is concerning, especially in the context of the ongoing Great Acceleration (Hooks, 2019; Steffen et al., 2015), where global human activities are accelerating due to economic growth aspirations (Meadows et al., 2017). Our results serve as a warning that a similar collapse could unfold among the bird populations of North America.

Is recruitment or loss the main component of the acceleration of bird population decline? We further demonstrate how changes in loss and recruitment rates contribute to the acceleration of bird population decline (Fig. 3e-f, Fig. 4). Loss of individuals is frequently linked to pollution (La Sorte et al., 2023; Liang et al., 2020), extreme events induced by climate change (Burthe et al., 2014), disease outbreaks (Chavatte et al., 2019; Lühken et al., 2017) or human disturbances (Fahrig & Rytwinski, 2009; Tryjanowski et al., 2015). In contrast, recruitment rate is directly linked to breeding success determined by the clutch size and successful fledges, and is driven by precipitation, habitat fragmentation, availability of nesting sites or food (Bennett et al., 2015; Cam & Aubry, 2011). Admittedly, extreme events, climatic fluctuations, disease outbreaks, and changes in land-use can impact both recruitment and loss of individuals, albeit with different relative magnitude. While we have not disentangled the relative importance of those drivers for the reported population declines and demographic rates, our results can help tailoring conservation policies and offer motivation and initial expectations for future experimental studies.

Decline in recruitment rates. Importantly, we have revealed a worrisome trend: 96% of species and 100% of families with increasing abundance are undergoing a decline in recruitment rates (Fig. 5). This suggests that most of the taxa with increasing abundance are, in fact, heading towards an eventual decline, should such a trend continue. Decrease in recruitment rate has been linked to habitat fragmentation (Robinson et al., 1995) or decrease in food abundance (Holmes & Sherry, 2001; Ponce et al., 2014), both of which have intensified since 1987 (Alofs & Fowler, 2010). Importantly, decrease in bird abundance is often seen as a direct result of the loss of individuals, and conservation policies often aim at directly reducing this loss. We show, however, that decreases in recruitment rate may themselves be responsible for significant population dynamics, stressing the importance of prioritizing increasing bird recruitment on par with preventing the loss. For instance, a decrease in the use of neonicotinoids (Hallmann et al., 2014; Li et al., 2020) or installation of nest boxes (Møller et al., 2014) are policies supporting recruitment, with a potential to bend the curve of a future recruitment collapse.

Using one of the most comprehensive local bird time series datasets in the world, coupled with a model disentangling processes of recruitment and loss, we provide insights into the abundance dynamics and their underlying processes of 508 species over 35 years across a continental scale. This marks a significant advancement, as we offer detailed insights into demographic dynamics that were previously unexplored for such a broad spectrum of species and at such an expansive spatial scale. Importantly, we reveal geographic hotspots of acceleration of bird abundance decline and attribute these declines to shifts of

recruitment and loss since 1987. We propose that regions with accelerated decline correspond to areas with high human populations and activities, which are themselves increasing at an accelerated pace. We also highlight a concerning trend: nearly every species with an increasing population is tending toward an eventual decline due to a ubiquitous decrease in recruitment rate. This is alarming, especially considering projections of exponential acceleration in human activities across various sectors such as economy, agriculture, or transportation, with no foreseeable reversal of this trend.

Methods

Data. To investigate the acceleration of bird decline in North America, we used the North American Breeding Bird Survey (Ziolkowski Jr. et al., 2022), an ongoing bird monitoring initiative launched in 1966. Spanning more than 50 years, the BBS comprises 39.2 km-long routes scattered across the contiguous United States and Canada, each divided into 50 census points at approximately 800 m intervals. From its inception with about 500 routes in 1966, the BBS has grown to encompass 5,581 routes by 2021. At the time of our data download on September 5, 2022, the data contained 6,946,871 records compiled by 10,316 volunteers for 746 species and spanning over 50 years. The BBS data also contain meteorological data, date, hour, and spatial coordinates.

Routes with long time-series (*e.g.* from 1969 to 2021) were spatially sparse. To balance long temporal extent with robust spatial coverage, we focused our analysis on the 1987-2021 period and selected routes with no more than 15 years of missing data.

For each species, we extracted the preferred habitat from the eBird/Cornell online database (Ziolkowski Jr. et al., 2022). These were: Towns, Grasslands, Shorelines, Scrubs, Deserts, Rivers and Streams, Marshes, Open Woodlands, Forests, Lakes and Ponds, Oceans, and Tundra. Species with missing habitat data (23 in total) were excluded. In the end, we performed our analysis using 1033 routes from 1987 to 2021 (*i.e.* 35 years), with 1,623,394 occurrences of 564 species.

Dynamic *N*-mixture model. We modelled the abundance of each of the 564 bird species across each route and year from 1987 to 2021 using a dynamic *N*-mixture model (Dail & Madsen, 2011), hereafter the DM model. It is a generalization of the *N*-mixture model by Royle (2004) that assumes open populations (*i.e.* metapopulations can experience births, recruitments, deaths, or emigrations).

For a species j and a route i, the abundance at time $t+1$ (*i.e.* $N_{j,i,t+1}$) is the sum of surviving ($S_{j,i,t+1}$) and recruited ($R_{j,i,t+1}$) individuals from time t:

$$N_{j,i,t+1} = S_{j,i,t+1} + R_{j,i,t+1} \qquad \text{eq. 1}$$

with survival $S_{j,i,t+1}$ and recruitment $R_{j,i,t+1}$ modelled as:

$$S_{j,i,t+1} \sim Binomial(N_{j,i,t}, \phi_{j,i,t}) \qquad \text{eq. 2}$$

$$R_{j,i,t+1} \sim Poisson(\gamma_{j,i,t}) \qquad \text{eq. 3}$$

$N_{j,i,t}$ is the abundance of species j at route i and time t, ϕ is the average probability of individual survival, and γ is the number of recruited individuals. The abundance at time 1 ($N_{j,i,1}$) is:

$$N_{j,i,1} \sim Poisson(\lambda_{j,i,1}), \text{eq. 4}$$

where λ is the mean abundance of the species at time 1.

The DM model corrects for imperfect detection, where the *observed* abundance ($n_{j,i,t}$) is corrected to estimate the true abundance ($N_{j,i,t}$):

$$n_{(j,i,t)} \sim Binomial\left(N_{j,i,t}, p_{j,i,t}\right) \text{ eq. 5}$$

$$\text{logit}\left(p_{j,i,t}\right) = \alpha + \boldsymbol{x}_{j,i,t}^{\intercal}\boldsymbol{b}, \qquad \text{eq. 6}$$

where p is the probability of detection of an individual, $\boldsymbol{x}^{\intercal}$ is the transpose of a vector of covariates, $\boldsymbol{b}$ is a vector of regression coefficients, and α is the intercept. $\boldsymbol{x}$ includes the exact time of the day of the census (in decimal hours), and weather data, *i.e.* wind condition (ordinal variable with 9 levels ranging from < 2 km.h^{-1} to 74 km.h^{-1}), sky condition (factor with 7 levels: clear sky, partly cloudy, cloudy, fog, drizzle, snow, and shower), and average temperature during the census (in °C). Missing values for the time of the day and temperature were imputed following Kéry and Royle (2015):

$$x_{i,t} \sim Normal(\mu, \sigma^2) \quad \text{eq. 7}$$

where $x_{i,t}$ is the imputed value of the covariate x at route i and time t, and μ and σ^2 are means and variances of the available data.

For each *j*-th species we fitted the DM model in a Bayesian framework using MCMC sampler JAGS (Plummer, 2003; https://mcmc-jags.sourceforge.io/), interfaced through the package jagsUI (Kellner, 2021) in R ver. 4.2.1 (R Core Team, 2021). For all the parameters, we used normal distributions with 0 mean and variance of 100 (Appendix B). The settings for the MCMC algorithm were: 3 chains, 100,000 iterations per chain, 75,000 burn-in, a thinning rate of 10, and 1,000 iterations in the adaptative phase. The entire fitting procedure for all 564 species (1 core per MCMC chain, 3 chains per species) required *ca.* 2 days on 1,692 cores of the Ohio Supercomputer (https://www.osc.edu/), each core operating at 2.5 GHz.

For each species, the DM models' convergence was assessed by computing the $\hat{R}$ (Rhat, Gelman & Rubin, 1992) for the main parameters (Appendix A: Fig. 4). To ensure to include as many species as possible, we visually inspected chain convergence and only models with $\hat{R} \leq 3$ for the main parameters. For abundance (N), survival (S) and recruitment (R), we excluded species for which the standard deviation was higher than the mean to control for absurd values. This led to a final set of 508 species for further analysis.

Rates of change. From the output of the DM model and for each *j*-th species at *i*-th site and *t*-th year (starting from 1988), we derived the yearly number of lost individuals L, as well as the per-capita growth rate g, per-capita recruitment rate r, and per-capita loss rate l:

$$L_{j,i,t+1} = N_{j,i,t} - S_{j,i,t+1} \qquad \text{eq. 8}$$

$$g_{j,i,t+1} = \frac{N_{j,i,t+1} - N_{j,i,t}}{N_{j,i,t}} = \frac{\Delta N}{N_t} \qquad \text{eq. 9}$$

$$r_{j,i,t+1} = \frac{R_{j,i,t+1}}{N_{j,i,t}} \qquad \text{eq. 10}$$

$$l_{j,i,t+1} = \frac{L_{j,i,t+1}}{N_{j,i,t}} \qquad \text{eq. 11}$$

Here, ΔN represents the change of abundance between time t and $t+1$. The average change of abundance over the time series, ΔN, was assessed as the slope of a linear regression between abundance N_t and year t:

$$N_t = \Delta N \times t + \beta_0 \qquad \text{eq. 12}$$

Additionally, we calculated the per-capita growth rate relative to the size of the initial population in 1987, hereafter relative growth rate g_{t1}, as:

$$g_{t1\,|\,j,i,t} = \frac{N_{j,i,t} - N_{j,i,1}}{N_{j,i,1}} \qquad \text{eq. 13}$$

We also assessed temporal change of g_{t1} (Δg_{t1}) using a linear regression:

$$g_{t1|t} = \Delta g_{t1} \times t + \beta_0 \quad \text{eq. 14}$$

Temporal change of yearly rates. We evaluated the temporal dynamics of per-capita rates. We denoted the temporal change of yearly growth rate as Δg, temporal change of loss rate as Δl, and temporal change of recruitment rate as Δr. These were assessed as slopes (Δy) of linear regressions of each metric y (where y is either g, l, or r) as a function of time t as:

$$y_i = \Delta y_i \times t + \beta_0\,, \qquad \text{eq. 15}$$

with β_0 the intercept. Since g is the per-capita change of population N over time, Δg is the acceleration or deceleration of ΔN (Fig. 1A).

Per route, per species, per family and per habitat analyses. We conducted the assessment of the temporal change in abundance (ΔN), temporal change in growth rate (Δg), temporal change in recruitment rate (Δr) and temporal change in loss rate (Δl) for different levels of aggregation.

First, we performed a spatial analysis. For each route i and each year t, we aggregated the number of individuals, recruitments, or losses of all the species together. Thus, we assessed the temporal change of this aggregated abundance (ΔN_i), temporal change in growth rate (Δg_i), temporal change in recruitment rate (Δr_i) and temporal change in loss rate (Δl_i), and we mapped these quantities geographically, either raw, or smoothened (see next section).

Second, we performed a temporal analysis at the species level, at the family level, and at the preferred habitat level. That is, for each j^{th}- species, or j^{th}- family, or j^{th}- habitat, we assessed the temporal change in abundance (ΔN_j), temporal change in growth rate (Δg_j), temporal change in recruitment rate (Δr_j) and temporal change in loss rate (Δl_j) at the North-American scale. In other words, these were not mapped geographically as in the spatial analysis, but the numbers were aggregated for each grouping (species, family, habitat) over all 1,033 routes included in our analysis.

Spatial smoothing. By mapping the above-mentioned temporal changes (ΔN, Δg, Δl, Δr), there could be a substantial local variation among individual routes, obscuring average trends across larger regions. To

detect these regional anomalies, we smoothened the variation of the rates using spatial generalized additive models (GAM) using the R package mgcv (Wood, 2011):

$$\Delta y_i = \mathrm{s}(Lon_i, Lat_i), \quad \text{eq. 16}$$

with Δy_i the temporal change of the metric considered at route i, Lon and Lat the longitude and latitude of the route i, and $s()$ indicating that longitude and latitude are treated as interacting covariates in the spline function of the smoother. For the spline function, we used a gaussian process as a smooth class (argument "bs" of the $s()$ function in mgcv) with 100 basis functions (*ca.* $\frac{1}{10}^{th}$ of the number of routes).

Classification of acceleration and deceleration. The same Δg value can emerge from different combinations of Δl and Δr; that is, acceleration or deceleration of ΔN can result from increases or decreases in per-capita loss, recruitment, or both. To capture this complexity, we devised a classification system for temporal population dynamics based on Δl and Δr (Fig. 1b, c), which allowed us to show the relative importance of Δl and Δr in a single map. We created a color scheme where each route (or species, family, or preferred habitat) lays in a 2-dimensional space with Δl on the x-axis and Δr on the y-axis (henceforth $\Delta l \Delta r$ space). For instance, our analysis reveals that at the route level, the average ΔN is negative (indicated by ↓). In this case, blue, and green hues indicate deceleration of population decline (Fig. 1C), which can be mainly attributed to either a negative Δl (blue) or to a positive Δr (green). Conversely, still in the case of a negative ΔN (↓), red and orange hues indicate an acceleration of the decline, and that either a positive Δl (red) or a negative Δr (orange) is the main component of the acceleration. This classification was applied to individual routes, as well as to smoothed averages. We note that for positive ΔN (indicate by ↑), implications of the color scheme are slightly different (*i.e.* either acceleration or deceleration of increasing population), but the interpretation about positive or negative Δr and Δl remains consistent.

References

Alofs, K. M., & Fowler, N. L. (2010). Habitat fragmentation caused by woody plant encroachment inhibits the spread of an invasive grass. *Journal of Applied Ecology*, *47*(2), 338–347. https://doi.org/10.1111/j.1365-2664.2010.01785.x

Barnosky, A. D., Matzke, N., Tomiya, S., Wogan, G. O. U., Swartz, B., Quental, T. B., Marshall, C., McGuire, J. L., Lindsey, E. L., Maguire, K. C., Mersey, B., & Ferrer, E. A. (2011). Has the Earth's sixth mass extinction already arrived? *Nature*, *471*(7336), Article 7336. https://doi.org/10.1038/nature09678

Bennett, J. M., Clarke, R. H., Thomson, J. R., & Mac Nally, R. (2015). Fragmentation, vegetation change and irruptive competitors affect recruitment of woodland birds. *Ecography*, *38*(2), 163–171. https://doi.org/10.1111/ecog.00936

Bowler, D. E., Heldbjerg, H., Fox, A. D., De Jong, M., & Böhning-Gaese, K. (2019). Long-term declines of European insectivorous bird populations and potential causes. *Conservation Biology*, *33*(5), 1120–1130. https://doi.org/10.1111/cobi.13307

Burthe, S., Wanless, S., Newell, M., Butler, A., & Daunt, F. (2014). Assessing the vulnerability of the marine bird community in the western North Sea to climate change and other anthropogenic impacts. *Marine Ecology Progress Series*, *507*, 277–295. https://doi.org/10.3354/meps10849

Cam, E., & Aubry, L. (2011). Early development, recruitment and life history trajectory in long-lived birds. *Journal of Ornithology*, *152*(S1), 187–201. https://doi.org/10.1007/s10336-011-0707-0

Ceballos, G., Ehrlich, P. R., Barnosky, A. D., García, A., Pringle, R. M., & Palmer, T. M. (2015). Accelerated modern human–induced species losses: Entering the sixth mass extinction. *Science Advances*, *1*(5), e1400253. https://doi.org/10.1126/sciadv.1400253

Chavatte, J.-M., Giraud, P., Esperet, D., Place, G., Cavalier, F., & Landau, I. (2019). An outbreak of trichomonosis in European greenfinches *Chloris chloris* and European goldfinches *Carduelis carduelis* wintering in Northern France. *Parasite*, *26*, 21. https://doi.org/10.1051/parasite/2019022

Chen, H., Hagerty, S., Crotty, S. M., & Bertness, M. D. (2016). Direct and indirect trophic effects of predator depletion on basal trophic levels. *Ecology*, *97*(2), 338–346. https://doi.org/10.1890/15-0900.1

Dail, D., & Madsen, L. (2011). Models for Estimating Abundance from Repeated Counts of an Open Metapopulation. *Biometrics*, *67*(2), 577–587. https://doi.org/10.1111/j.1541-0420.2010.01465.x

Daskalova, G. N., Myers-Smith, I. H., & Godlee, J. L. (2020). Rare and common vertebrates span a wide spectrum of population trends. *Nature Communications*, *11*(1), 4394. https://doi.org/10.1038/s41467-020-17779-0

Díaz, S., Settele, J., Brondízio, E. S., Ngo, H. T., Agard, J., Arneth, A., Balvanera, P., Brauman, K. A., Butchart, S. H. M., Chan, K. M. A., Garibaldi, L. A., Ichii, K., Liu, J., Subramanian, S. M., Midgley, G. F., Miloslavich, P., Molnár, Z., Obura, D., Pfaff, A., … Zayas, C. N. (2019). Pervasive human-driven decline of life on Earth points to the need for transformative change. *Science*, *366*(6471), eaax3100. https://doi.org/10.1126/science.aax3100

Dornelas, M., Chase, J. M., Gotelli, N. J., Magurran, A. E., McGill, B. J., Antão, L. H., Blowes, S. A., Daskalova, G. N., Leung, B., Martins, I. S., Moyes, F., Myers-Smith, I. H., Thomas, C. D., & Vellend, M. (2023). Looking back on biodiversity change: Lessons for the road ahead. *Philosophical Transactions of the Royal Society B: Biological Sciences*, *378*(1881), 20220199. https://doi.org/10.1098/rstb.2022.0199

Fahrig, L., & Rytwinski, T. (2009). Effects of Roads on Animal Abundance: An Empirical Review and Synthesis. *Ecology and Society*, *14*(1), art21. https://doi.org/10.5751/ES-02815-140121

Fraixedas, S., Lindén, A., Meller, K., Lindström, Å., Keišs, O., Kålås, J. A., Husby, M., Leivits, A., Leivits, M., & Lehikoinen, A. (2017). Substantial decline of Northern European peatland bird populations: Consequences of drainage. *Biological Conservation*, *214*, 223–232. https://doi.org/10.1016/j.biocon.2017.08.025

Frank, K. T., Petrie, B., Choi, J. S., & Leggett, W. C. (2005). Trophic Cascades in a Formerly Cod-Dominated Ecosystem. *Science*, *308*(5728), 1621–1623. https://doi.org/10.1126/science.1113075

Freckleton, R. P. (2011). Dealing with collinearity in behavioural and ecological data: Model averaging and the problems of measurement error. *Behavioral Ecology and Sociobiology*, *65*(1), 91–101. https://doi.org/10.1007/s00265-010-1045-6

Gelman, A., & Rubin, D. B. (1992). Inference from Iterative Simulation Using Multiple Sequences. *Statistical Science*, *7*(4). https://doi.org/10.1214/ss/1177011136

Green, R. E., Cornell, S. J., Scharlemann, J. P. W., & Balmford, A. (2005). Farming and the Fate of Wild Nature. *Science*, *307*(5709), 550–555. https://doi.org/10.1126/science.1106049

Hallmann, C. A., Foppen, R. P. B., Van Turnhout, C. A. M., De Kroon, H., & Jongejans, E. (2014). Declines in insectivorous birds are associated with high neonicotinoid concentrations. *Nature*, *511*(7509), 341–343. https://doi.org/10.1038/nature13531

Holmes, R. T., & Sherry, T. W. (2001). Thirty-Year Bird Population Trends in an Unfragmented Temperate Deciduous Forest: Importance of Habitat Change. *The Auk*, *118*(3), 589–609. https://doi.org/10.1093/auk/118.3.589

Hooks, G. (Ed.). (2019). 7. Land Use and the Great Acceleration in Human Activities: Political and Economic Dynamics. In *The Sociology of Development Handbook* (pp. 190–206). University of California Press. https://doi.org/10.1525/9780520963474-009

Inger, R., Gregory, R., Duffy, J. P., Stott, I., Voříšek, P., & Gaston, K. J. (2015). Common European birds are declining rapidly while less abundant species' numbers are rising. *Ecology Letters*, *18*(1), 28–36. https://doi.org/10.1111/ele.12387

IPBES. (2019). *Global assessment report on biodiversity and ecosystem services of the Intergovernmental Science-Policy Platform on Biodiversity and Ecosystem Services* (Version 1). Zenodo. https://doi.org/10.5281/ZENODO.3831673

Jackson, J. B. C., Kirby, M. X., Berger, W. H., Bjorndal, K. A., Botsford, L. W., Bourque, B. J., Bradbury, R. H., Cooke, R., Erlandson, J., Estes, J. A., Hughes, T. P., Kidwell, S., Lange, C. B., Lenihan, H. S., Pandolfi, J. M., Peterson, C. H., Steneck, R. S., Tegner, M. J., & Warner, R. R. (2001). Historical Overfishing and the Recent Collapse of Coastal Ecosystems. *Science*, *293*(5530), 629–637. https://doi.org/10.1126/science.1059199

Johnson, T. F., Beckerman, A. P., Childs, D. Z., Webb, T. J., Evans, K. L., Griffiths, C. A., Capdevila, P., Clements, C. F., Besson, M., Gregory, R. D., Thomas, G. H., Delmas, E., & Freckleton, R. P. (2024). Revealing uncertainty in the status of biodiversity change. *Nature*. https://doi.org/10.1038/s41586-024-07236-z

Kellner, K. (2021). *jagsUI: A Wrapper Around "rjags" to Streamline "JAGS" Analyses*. https://CRAN.R-project.org/package=jagsUI

Kéry, M., & Royle, J. A. (2015). *Applied Hierarchical Modeling in Ecology: Analysis of distribution, abundance and species richness in R and BUGS: Volume 1:Prelude and Static Models* (1st edition). Academic Press.

Kéry, M., & Royle, J. A. (2020). *Applied Hierarchical Modeling in Ecology: Analysis of Distribution, Abundance and Species Richness in R and BUGS: Volume 2: Dynamic and Advanced Models* (1st edition). Academic Press.

La Sorte, F. A., Lepczyk, C. A., & Aronson, M. F. J. (2023). Light pollution enhances ground-level exposure to airborne toxic chemicals for nocturnally migrating passerines. *Global Change Biology*, *29*(1), 57–68. https://doi.org/10.1111/gcb.16443

Leung, B., Greenberg, D. A., & Green, D. M. (2017). Trends in mean growth and stability in temperate vertebrate populations. *Diversity and Distributions*, *23*(12), 1372–1380. https://doi.org/10.1111/ddi.12636

Leung, B., Hargreaves, A. L., Greenberg, D. A., McGill, B., Dornelas, M., & Freeman, R. (2020). Clustered versus catastrophic global vertebrate declines. *Nature*, *588*(7837), 267–271. https://doi.org/10.1038/s41586-020-2920-6

Li, Y., Miao, R., & Khanna, M. (2020). Neonicotinoids and decline in bird biodiversity in the United States. *Nature Sustainability*, *3*(12), 1027–1035. https://doi.org/10.1038/s41893-020-0582-x

Liang, Y., Rudik, I., Zou, E. Y., Johnston, A., Rodewald, A. D., & Kling, C. L. (2020). Conservation cobenefits from air pollution regulation: Evidence from birds. *Proceedings of the National Academy of Sciences*, *117*(49), 30900–30906. https://doi.org/10.1073/pnas.2013568117

Lühken, R., Jöst, H., Cadar, D., Thomas, S. M., Bosch, S., Tannich, E., Becker, N., Ziegler, U., Lachmann, L., & Schmidt-Chanasit, J. (2017). Distribution of Usutu Virus in Germany and Its Effect on Breeding Bird Populations. *Emerging Infectious Diseases*, *23*(12), 1994–2001. https://doi.org/10.3201/eid2312.171257

Meadows, D. H., Randers, J., & Meadows, D. L. (2017). The Limits to Growth (1972). In L. Robin, S. Sörlin, & P. Warde (Eds.), *The Future of Nature* (pp. 101–116). Yale University Press. https://doi.org/10.12987/9780300188479-012

Møller, A. P., Adriaensen, F., Artemyev, A., Bańbura, J., Barba, E., Biard, C., Blondel, J., Bouslama, Z., Bouvier, J., Camprodon, J., Cecere, F., Chaine, A., Charmantier, A., Charter, M., Cichoń, M., Cusimano, C., Czeszczewik, D., Doligez, B., Doutrelant, C., … Lambrechts, M. M. (2014). Clutch-size variation in Western Palaearctic secondary hole-nesting passerine birds in relation to nest box design. *Methods in Ecology and Evolution*, *5*(4), 353–362. https://doi.org/10.1111/2041-210X.12160

Newbold, T., Tittensor, D. P., Harfoot, M. B. J., Scharlemann, J. P. W., & Purves, D. W. (2020). Non-linear changes in modelled terrestrial ecosystems subjected to perturbations. *Scientific Reports*, *10*(1), 14051. https://doi.org/10.1038/s41598-020-70960-9

Newton, I. (2004). The recent declines of farmland bird populations in Britain: An appraisal of causal factors and conservation actions. *Ibis*, *146*(4), 579–600. https://doi.org/10.1111/j.1474-919X.2004.00375.x

Piketty, T. (2014). *Capital in the Twenty-First Century*. Harvard University Press. https://doi.org/10.4159/9780674369542

Pilotto, F., Kühn, I., Adrian, R., Alber, R., Alignier, A., Andrews, C., Bäck, J., Barbaro, L., Beaumont, D., Beenaerts, N., Benham, S., Boukal, D. S., Bretagnolle, V., Camatti, E., Canullo, R., Cardoso, P. G., Ens, B. J., Everaert, G., Evtimova, V., … Haase, P. (2020). Meta-analysis of multidecadal biodiversity trends in Europe. *Nature Communications*, *11*(1), 3486. https://doi.org/10.1038/s41467-020-17171-y

Plummer, M. (2003). *JAGS: A program for analysis of Bayesian graphical models using Gibbs sampling. In K. Hornik, F. Leisch, & A. Zeileis (Eds.), Proceedings of the 3rd International Workshop on Distributed Statistical Computing, 124(125.10), 1–10.*

Ponce, C., Bravo, C., & Alonso, J. C. (2014). Effects of agri-environmental schemes on farmland birds: Do food availability measurements improve patterns obtained from simple habitat models? *Ecology and Evolution*, *4*(14), 2834–2847. https://doi.org/10.1002/ece3.1125

R Core Team. (2021). *R: A Language and Environment for Statistical Computing*. R Foundation for Statistical Computing. https://www.R-project.org/

Reid, N., Brommer, J. E., Stenseth, N. C., Marnell, F., McDonald, R. A., & Montgomery, W. I. (2021). Regime shift tipping point in hare population collapse associated with climatic and agricultural change during the very early 20th century. *Global Change Biology*, *27*(16), 3732–3740. https://doi.org/10.1111/gcb.15652

Rigal, S., Dakos, V., Alonso, H., Auniņš, A., Benkő, Z., Brotons, L., Chodkiewicz, T., Chylarecki, P., de Carli, E., del Moral, J. C., Domșa, C., Escandell, V., Fontaine, B., Foppen, R., Gregory, R., Harris, S., Herrando, S., Husby, M., Ieronymidou, C., … Devictor, V. (2023). Farmland practices are driving bird population decline across Europe. *Proceedings of the National Academy of Sciences*, *120*(21), e2216573120. https://doi.org/10.1073/pnas.2216573120

Robinson, S. K., Thompson, F. R., Donovan, T. M., Whitehead, D. R., & Faaborg, J. (1995). Regional Forest Fragmentation and the Nesting Success of Migratory Birds. *Science*, *267*(5206), 1987–1990. https://doi.org/10.1126/science.267.5206.1987

Rosenberg, K. V., Dokter, A. M., Blancher, P. J., Sauer, J. R., Smith, A. C., Smith, P. A., Stanton, J. C., Panjabi, A., Helft, L., Parr, M., & Marra, P. P. (2019). Decline of the North American avifauna. *Science*, *366*(6461), 120–124. https://doi.org/10.1126/science.aaw1313

Royle, J. A. (2004). N-Mixture Models for Estimating Population Size from Spatially Replicated Counts. *Biometrics*, *60*(1), 108–115. https://doi.org/10.1111/j.0006-341X.2004.00142.x

Stanton, R. L., Morrissey, C. A., & Clark, R. G. (2018). Analysis of trends and agricultural drivers of farmland bird declines in North America: A review. *Agriculture, Ecosystems & Environment*, *254*, 244–254. https://doi.org/10.1016/j.agee.2017.11.028

Steffen, W., Broadgate, W., Deutsch, L., Gaffney, O., & Ludwig, C. (2015). The trajectory of the Anthropocene: The Great Acceleration. *The Anthropocene Review*, *2*(1), 81–98. https://doi.org/10.1177/2053019614564785

Tryjanowski, P., Skórka, P., Sparks, T. H., Biaduń, W., Brauze, T., Hetmański, T., Martyka, R., Indykiewicz, P., Myczko, Ł., Kunysz, P., Kawa, P., Czyż, S., Czechowski, P., Polakowski, M., Zduniak, P., Jerzak, L., Janiszewski, T., Goławski, A., Duduś, L., … Wysocki, D. (2015). Urban and rural habitats differ in number and type of bird feeders and in bird species consuming supplementary food. *Environmental Science and Pollution Research*, *22*(19), 15097–15103. https://doi.org/10.1007/s11356-015-4723-0

Urban, M. C. (2015). Accelerating extinction risk from climate change. *Science*, *348*(6234), 571–573. https://doi.org/10.1126/science.aaa4984

Van Klink, R., Bowler, D. E., Gongalsky, K. B., Swengel, A. B., Gentile, A., & Chase, J. M. (2020). Meta-analysis reveals declines in terrestrial but increases in freshwater insect abundances. *Science*, *368*(6489), 417–420. https://doi.org/10.1126/science.aax9931

Wood, S. N. (2011). Fast stable restricted maximum likelihood and marginal likelihood estimation of semiparametric generalized linear models. *Journal of the Royal Statistical Society (B)*, *73*(1), 3–36.

Yan, L., & Roy, D. P. (2016). Conterminous United States crop field size quantification from multi-temporal Landsat data. *Remote Sensing of Environment*, *172*, 67–86. https://doi.org/10.1016/j.rse.2015.10.034

Ziolkowski Jr., D., Lutmerding, M., Aponte, V., & Hudson, M.-A. (2022). *2022 Release—North American Breeding Bird Survey Dataset (1966-2021)* [Csv]. U.S. Geological Survey. https://doi.org/10.5066/P97WAZE5

Supplementary information. Data, scripts, and figures are available on the following GitHub repository: https://github.com/FrsLry/ms_acceleration.

Acknowledgements. This study stands on the shoulders of the thousands of volunteers who participated in the North American BBS, and the institutions that manage this program. F.L. and P.K. were funded by the European Union (ERC, BEAST, 101044740). Views and opinions expressed are however those of the author(s) only and do not necessarily reflect those of the European Union or the European Research Council Executive Agency. Neither the European Union nor the granting authority can be held responsible

for them. M.A.J. was supported by the National Science Foundation DEB-1926598. The authors thank the Ohio Supercomputer Center for their computational resources.

Author Contributions. F.L. performed the statistical analysis. F.L, M.J., and P.K. wrote the paper.

Competing interest. The authors declare no competing financial interests.

Author information. Correspondence and requests for materials should be addressed to F.L. (leroy@fzp.czu.cz).

a

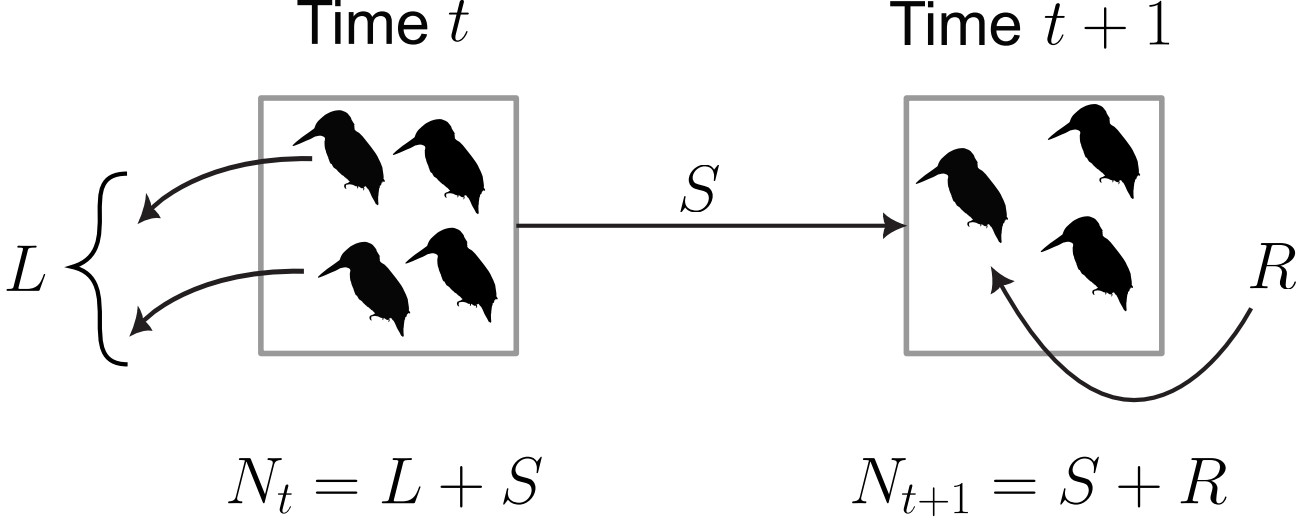

$$\Delta N = N_{t+1} - N_t = R - L$$

$$g = \frac{\Delta N}{N_t} = \frac{R}{N_t} - \frac{L}{N_t} = r - l$$

$$\Delta g = \Delta r - \Delta l = \Delta(\frac{\Delta N}{N_t})$$

b

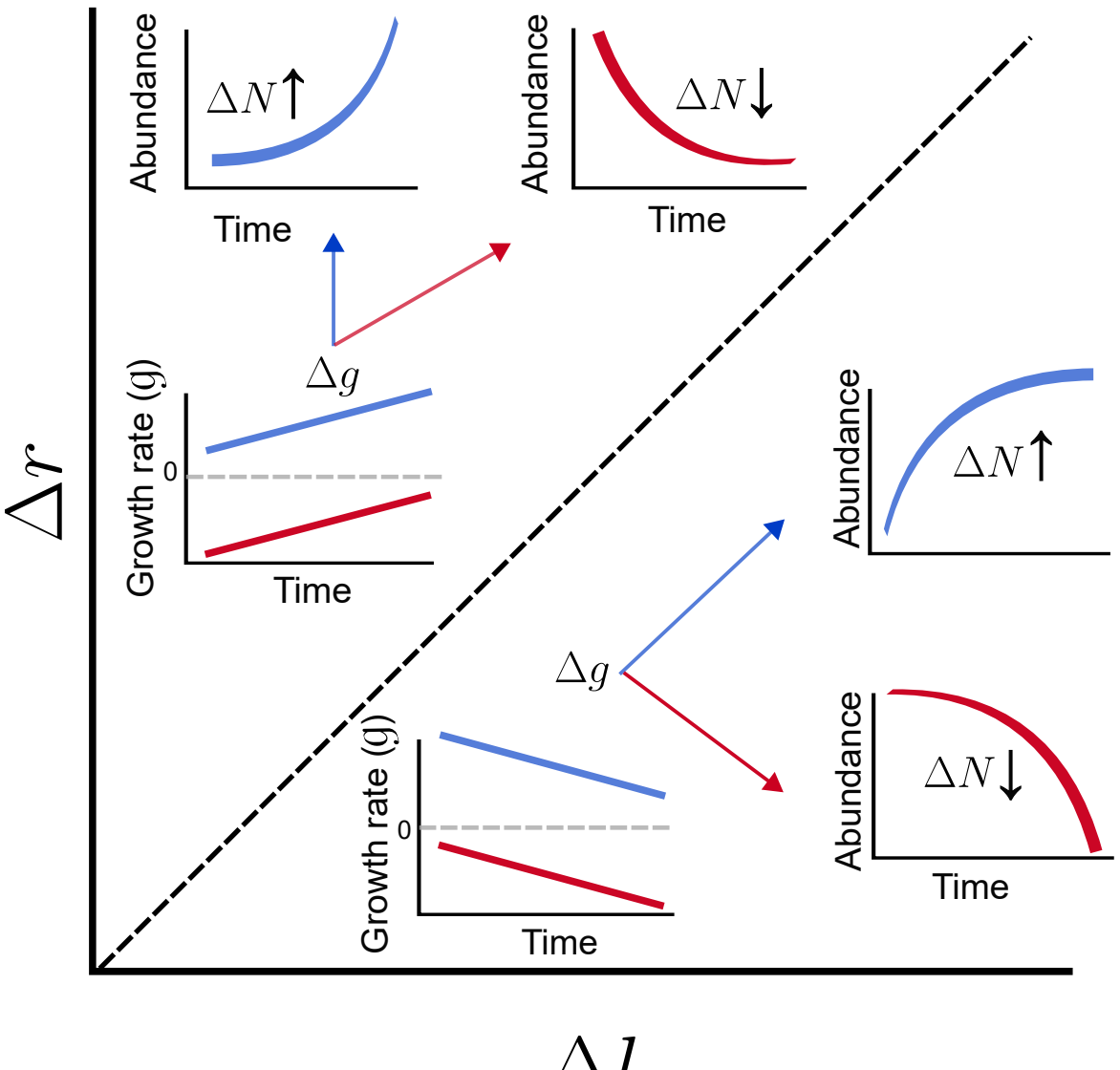

c

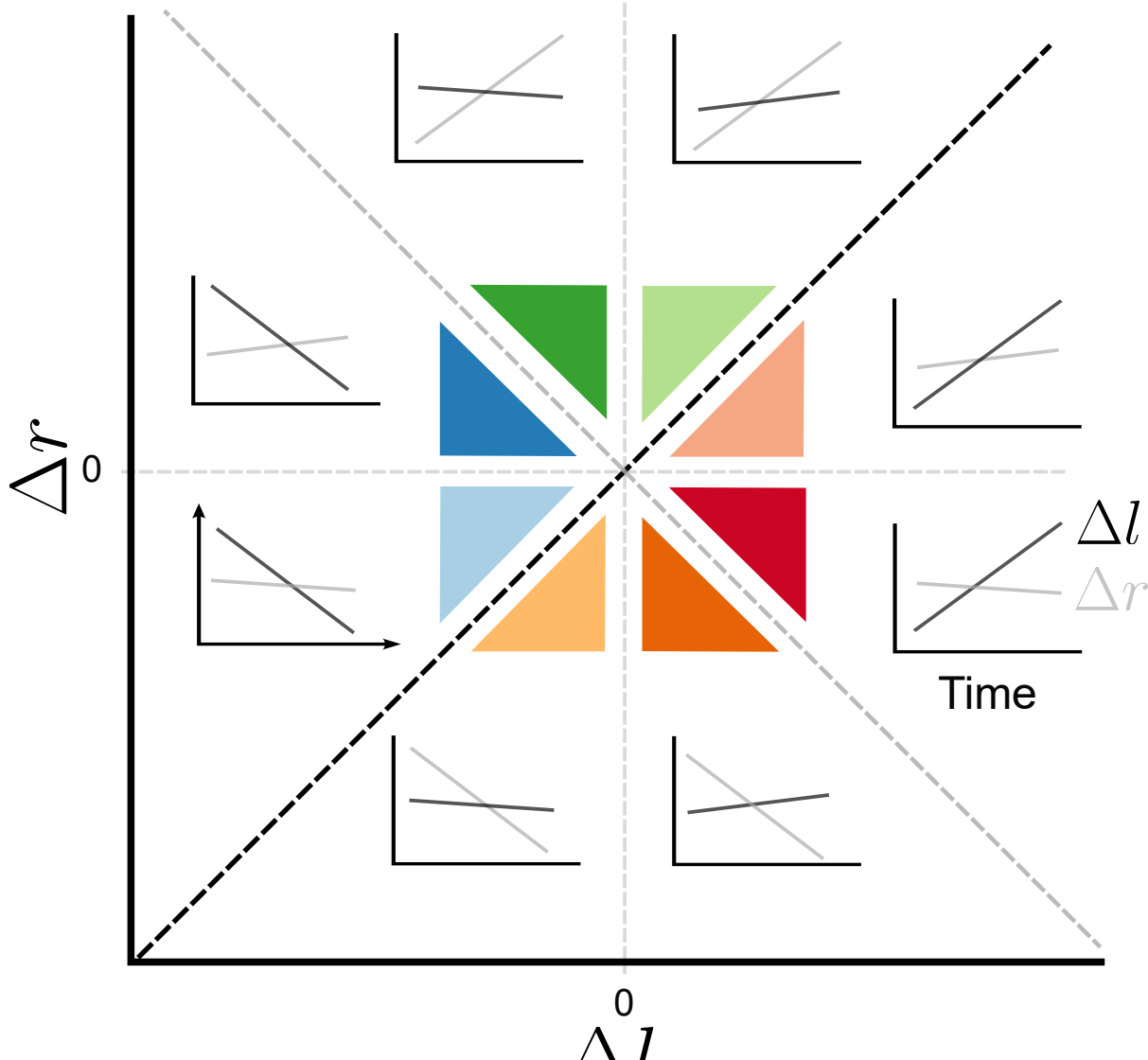

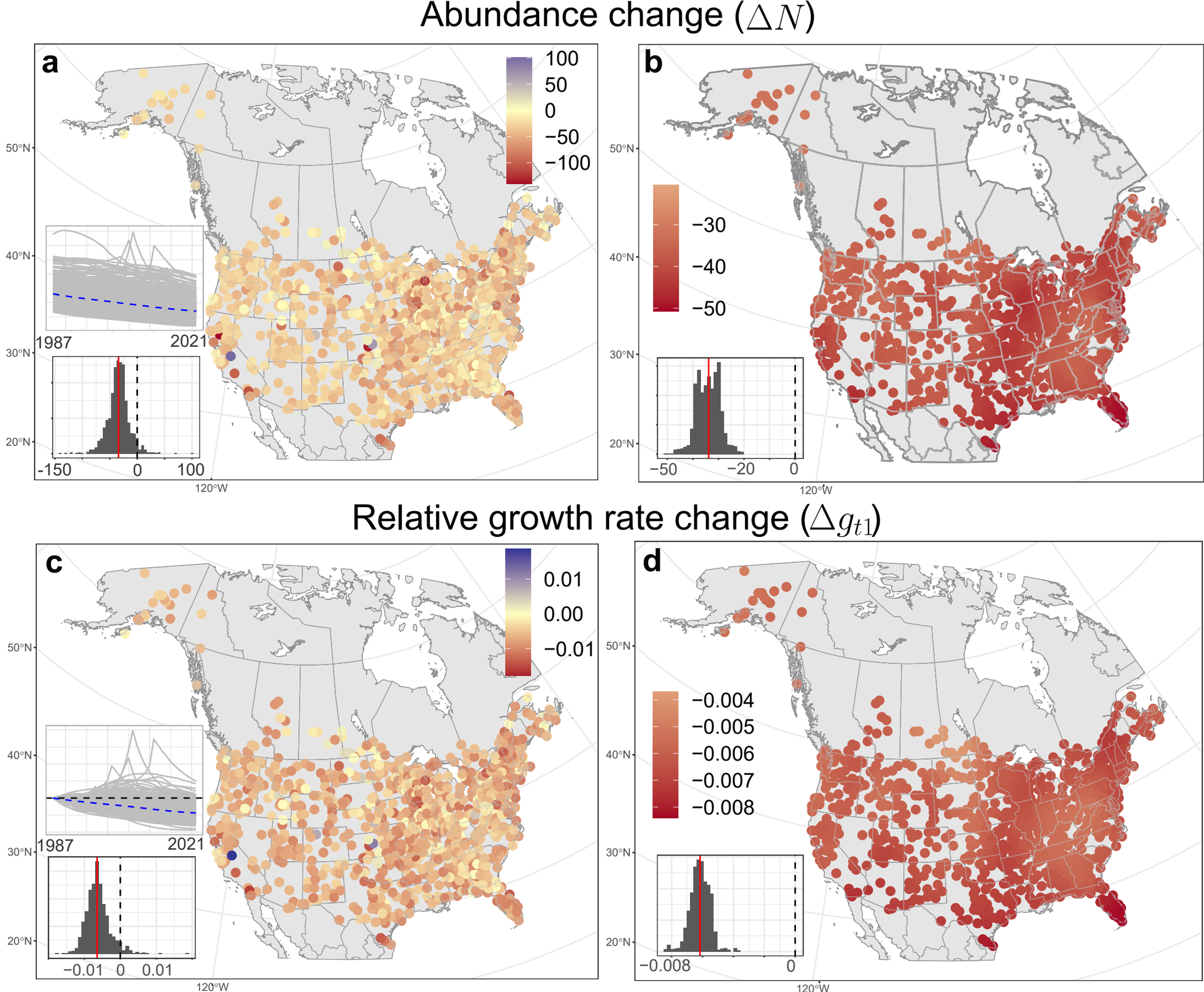
Abundance change (ΔN)
a
100
50
0
−50
−100
1987
2021
-150
0
100
50°N
40°N
30°N
20°N
120°W
b
−30
−40
−50
−50
−20
0
Relative growth rate change (Δg_{t1})
c
0.01
0.00
−0.01
−0.01
0
0.01
d
−0.004
−0.005
−0.006
−0.007
−0.008
−0.008
0

Growth rate change ($\triangle g$)

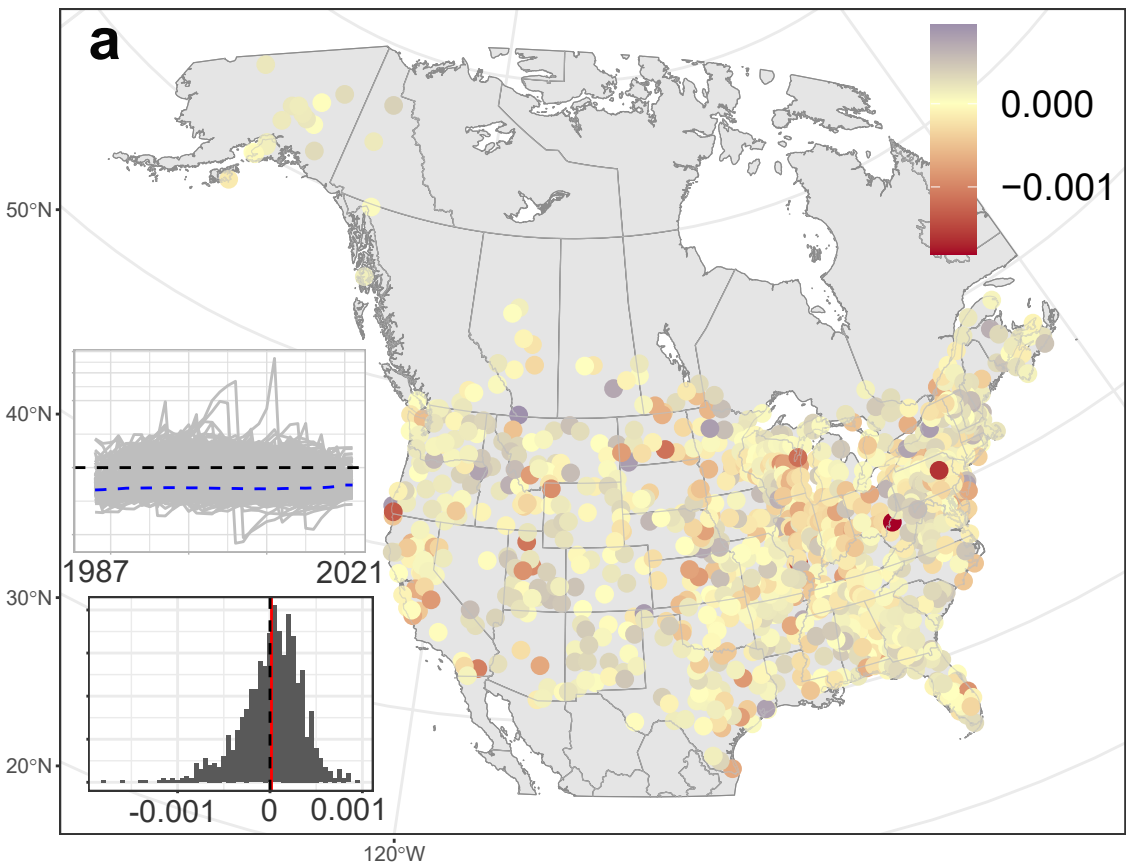

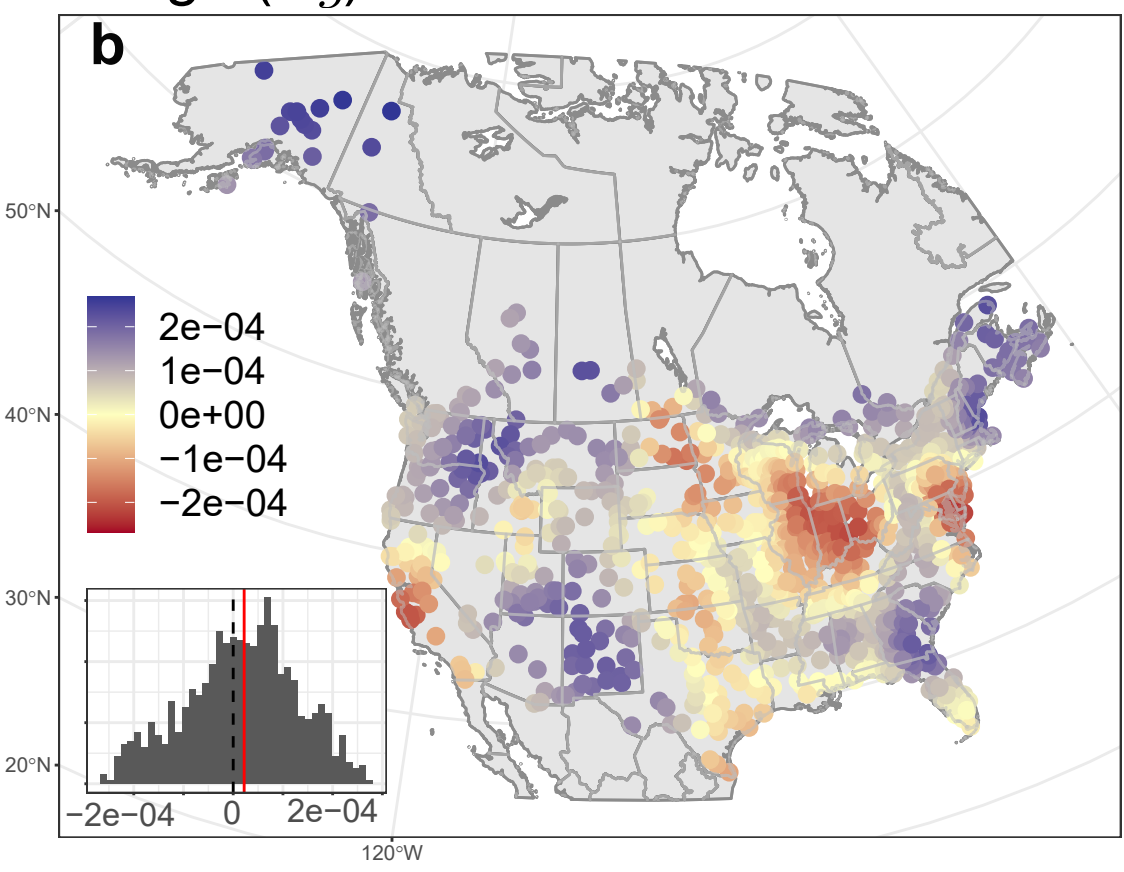

Recruitment rate change ($\triangle r$)

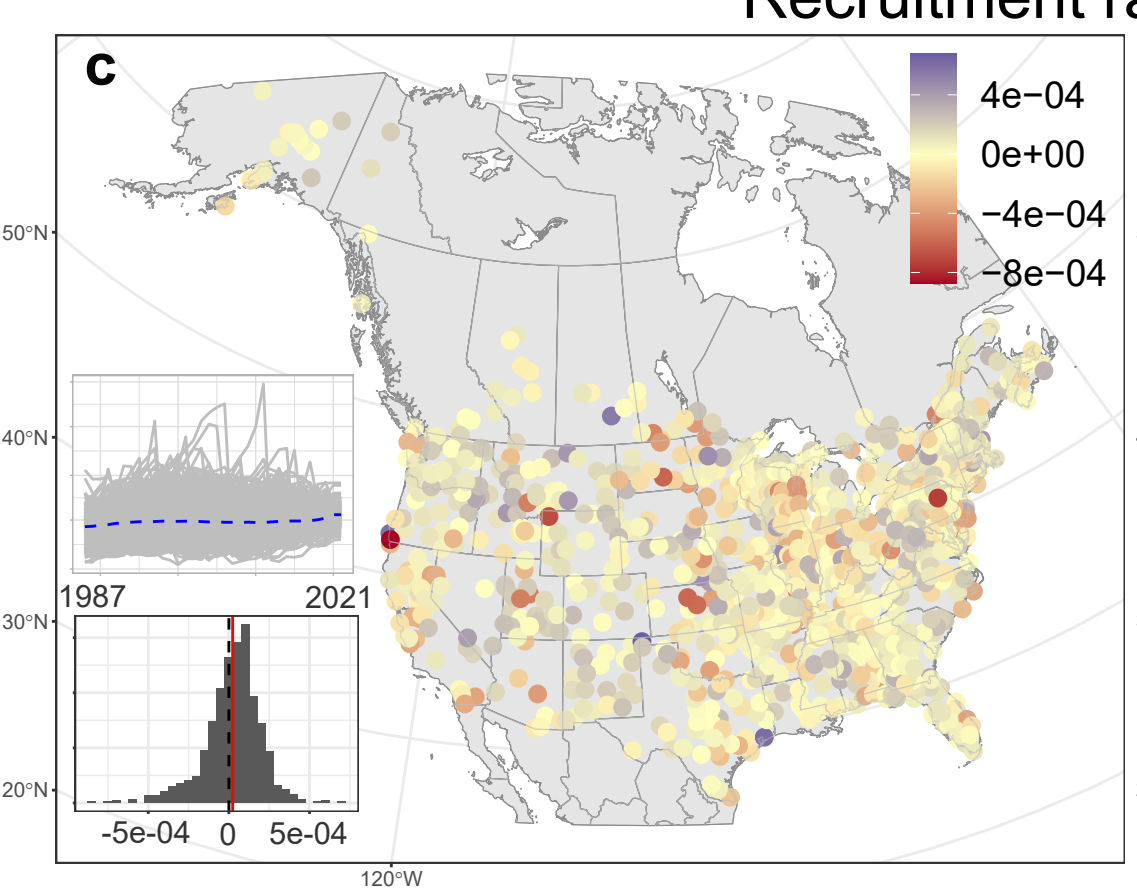

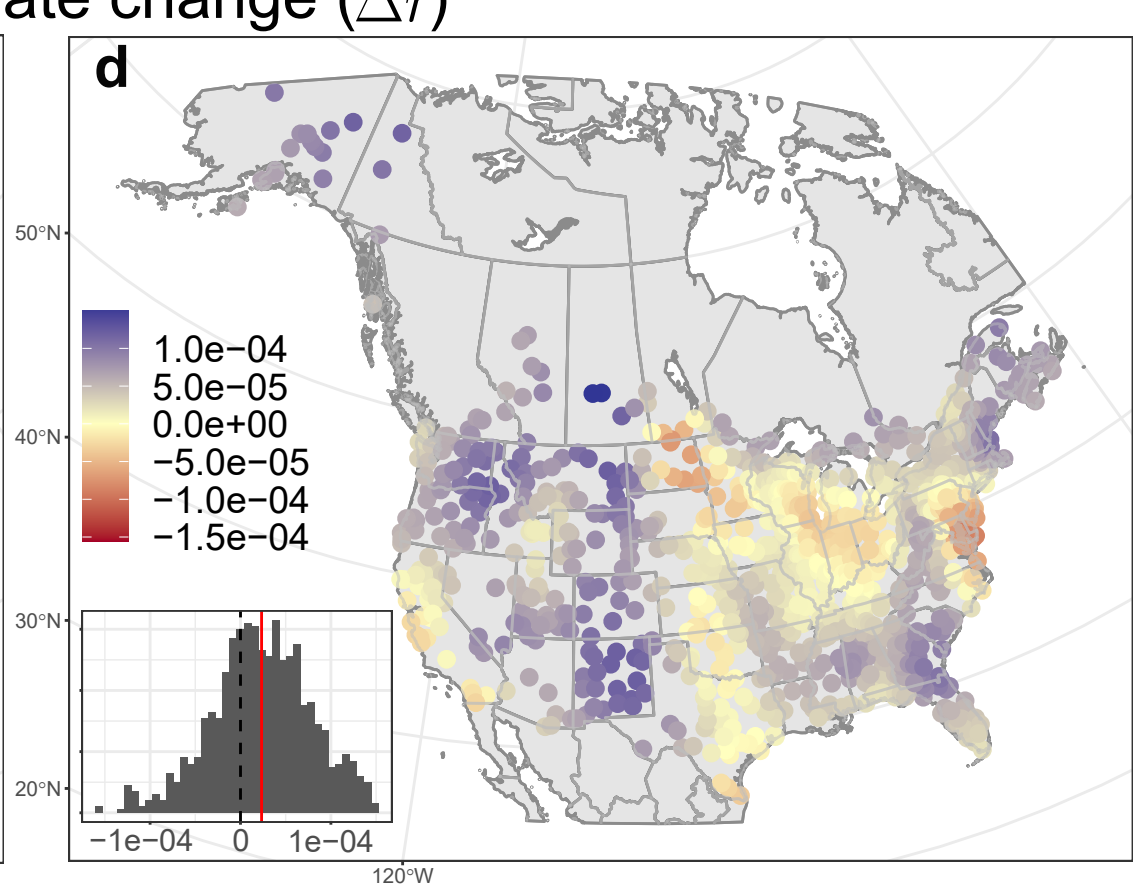

Loss rate change ($\triangle l$)

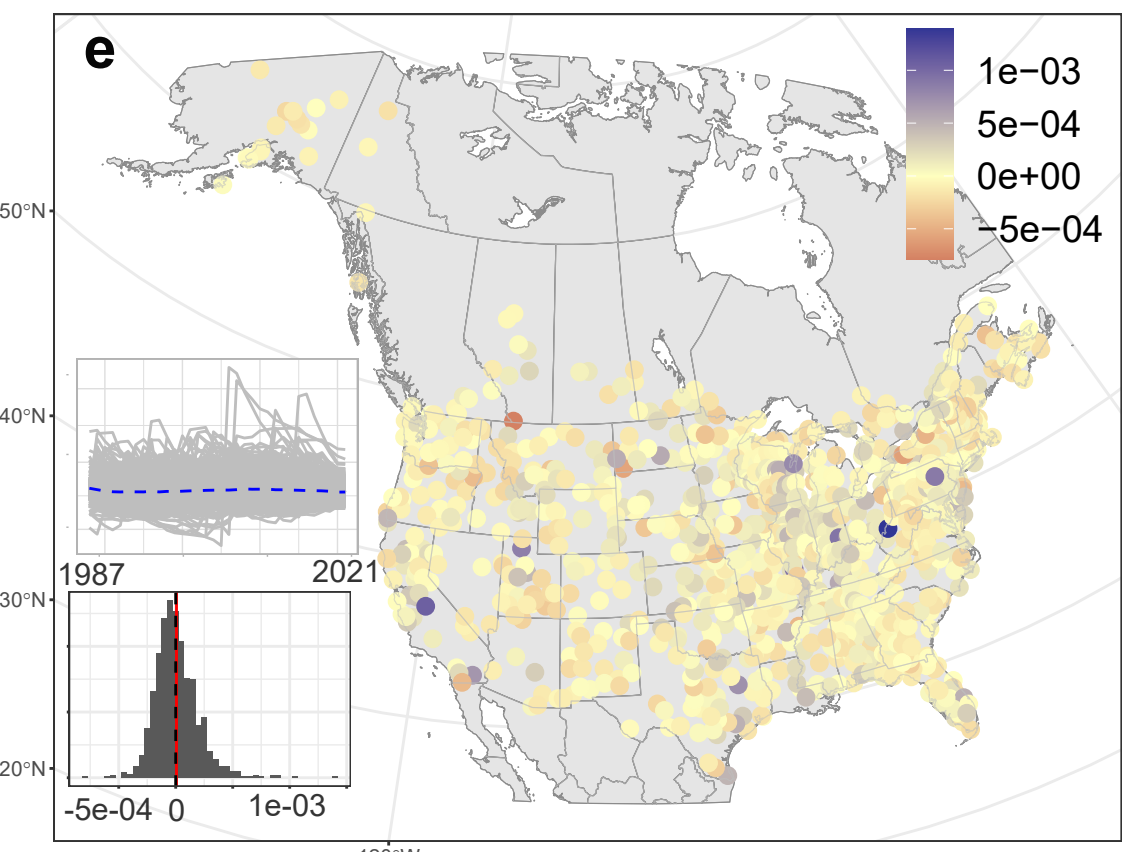

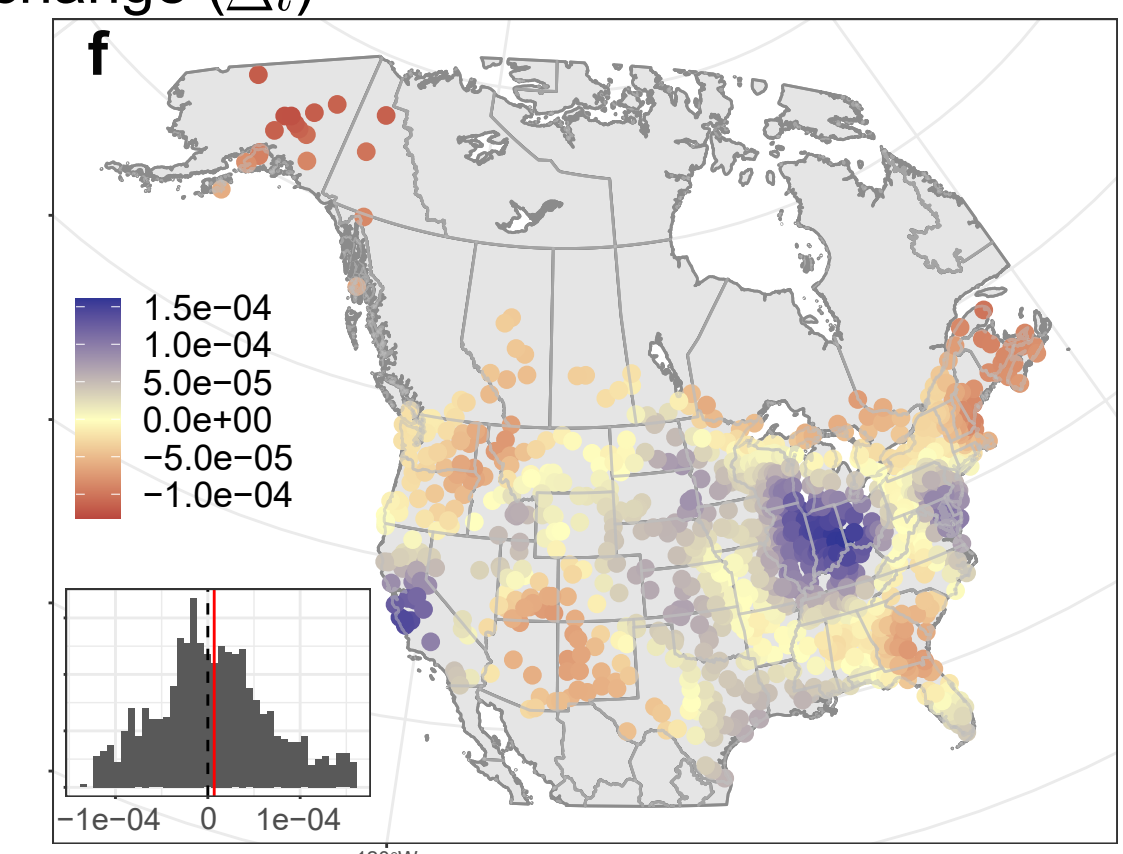

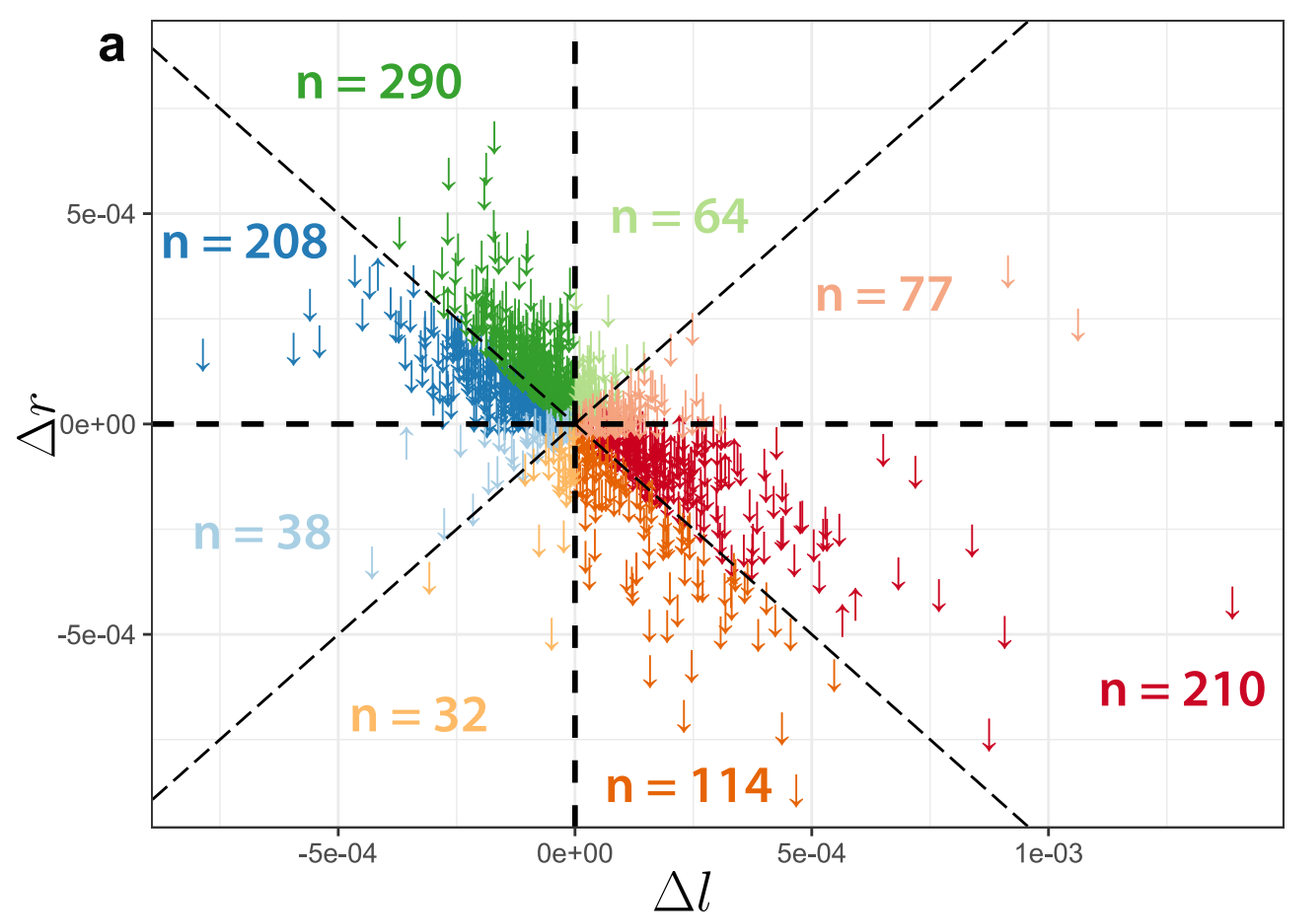
a
n = 290
n = 208
n = 64
n = 77
n = 38
n = 32
n = 114
n = 210
5e-04
0e+00
-5e-04
Δr
-5e-04
0e+00
5e-04
1e-03
Δl

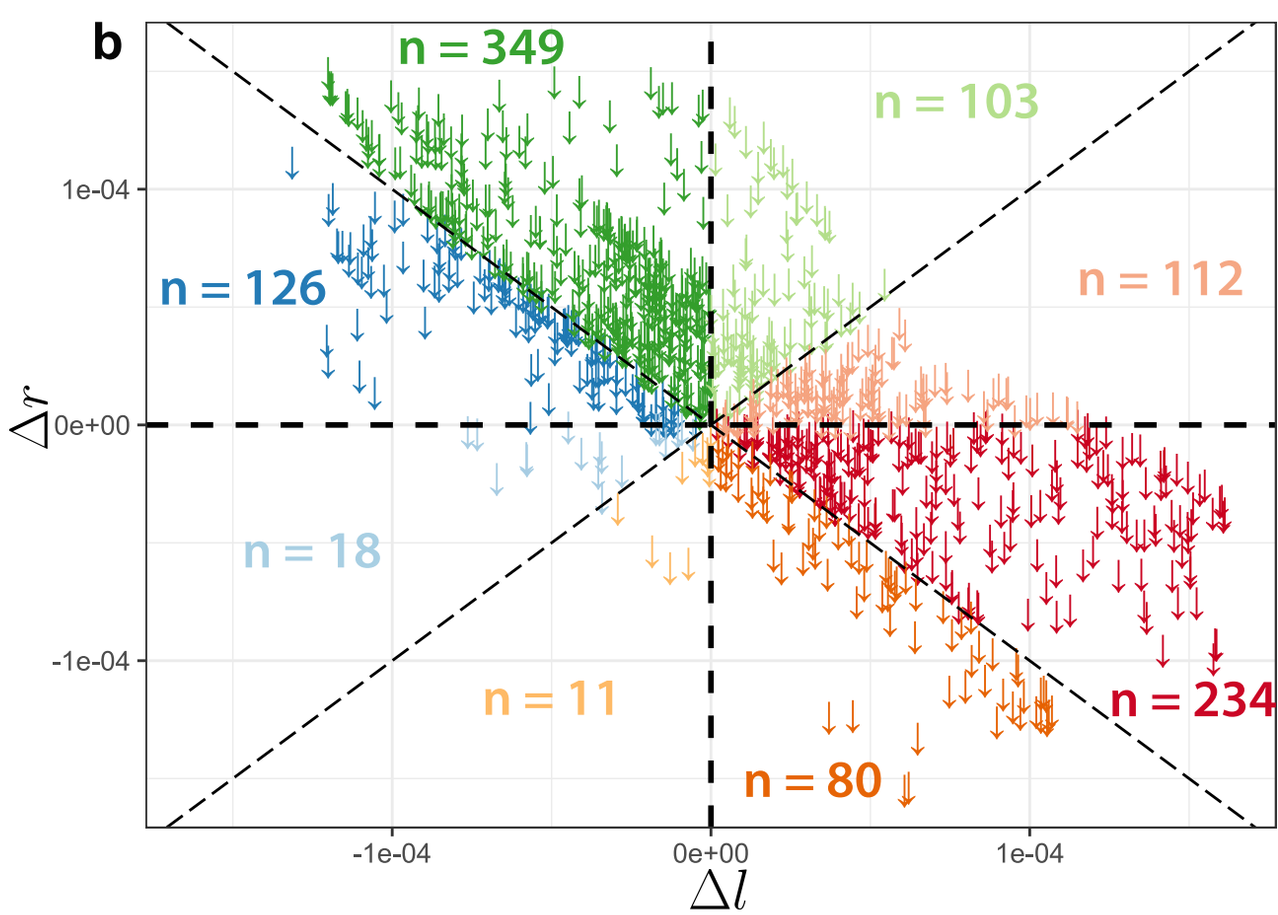
b
n = 349
n = 103
n = 126
n = 112
n = 18
n = 11
n = 80
n = 234
1e-04
0e+00
-1e-04
Δr
-1e-04
0e+00
1e-04
Δl

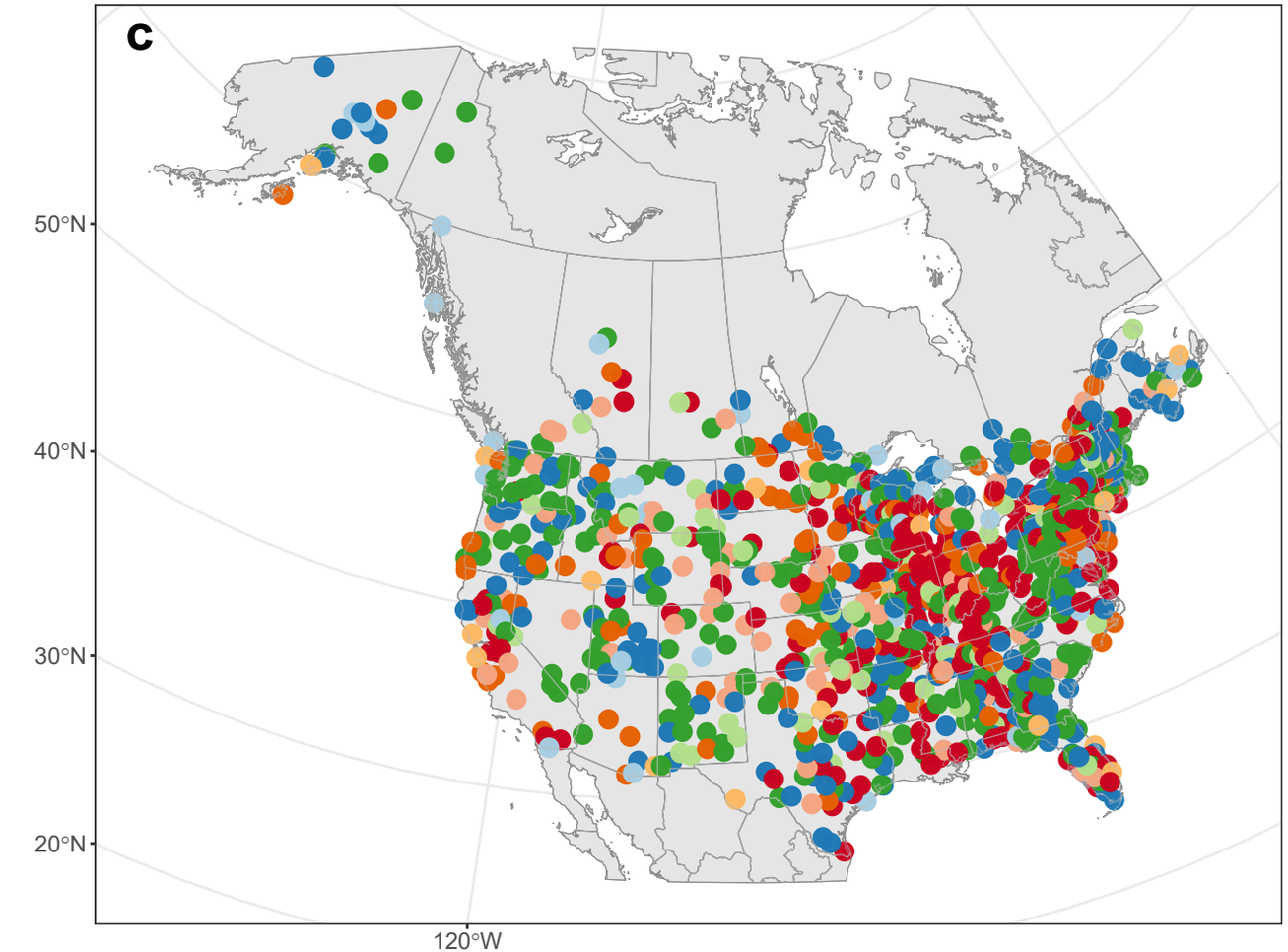
c
50°N
40°N
30°N
20°N
120°W

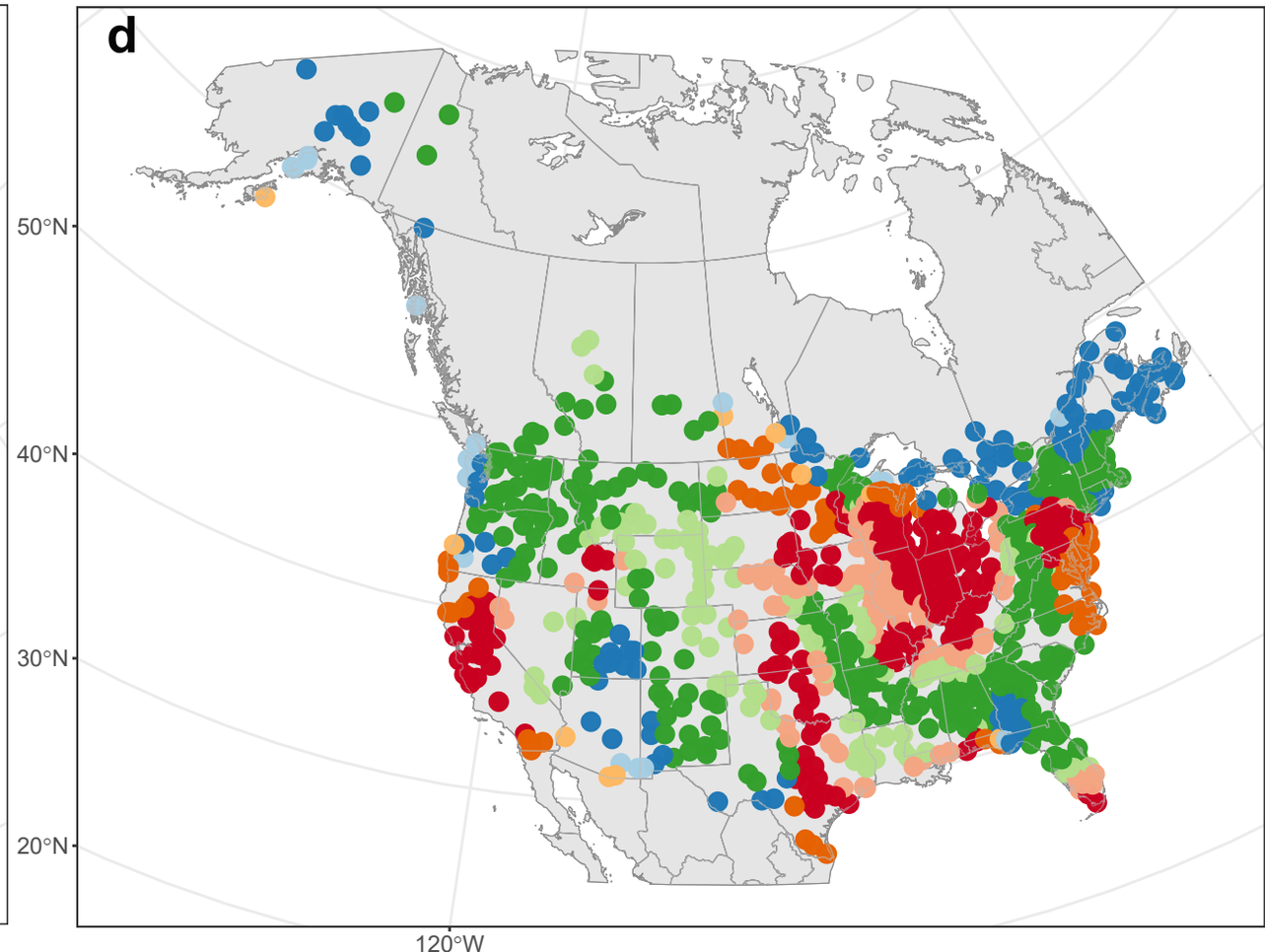
d
50°N
40°N
30°N
20°N
120°W

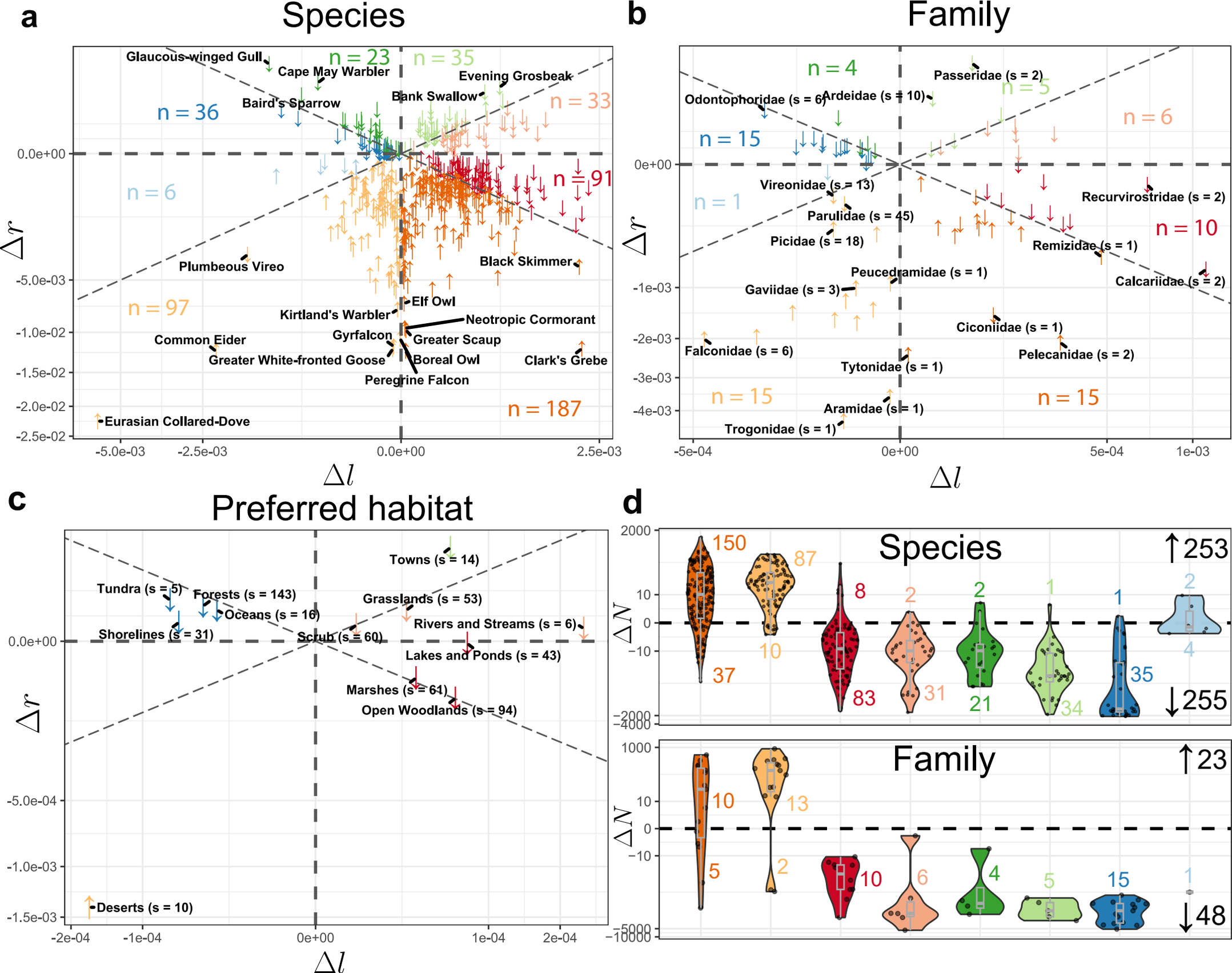
a
Species
Glaucous-winged Gull
Cape May Warbler
Evening Grosbeak
Bank Swallow
Baird's Sparrow
n = 23
n = 35
n = 36
n = 33
n = 91
n = 6
n = 97
n = 187
Plumbeous Vireo
Black Skimmer
Elf Owl
Kirtland's Warbler
Neotropic Cormorant
Gyrfalcon
Common Eider
Greater Scaup
Greater White-fronted Goose
Boreal Owl
Clark's Grebe
Peregrine Falcon
Eurasian Collared-Dove
0.0e+00
-5.0e-03
-1.0e-02
-1.5e-02
-2.0e-02
-2.5e-02
-5.0e-03
-2.5e-03
0.0e+00
2.5e-03
Δr
Δl
b
Family
n = 4
n = 5
n = 15
n = 6
n = 1
n = 10
n = 15
n = 15
Odontophoridae (s = 6)
Ardeidae (s = 10)
Passeridae (s = 2)
Vireonidae (s = 13)
Recurvirostridae (s = 2)
Parulidae (s = 45)
Picidae (s = 18)
Remizidae (s = 1)
Peucedramidae (s = 1)
Calcariidae (s = 2)
Gaviidae (s = 3)
Ciconiidae (s = 1)
Falconidae (s = 6)
Pelecanidae (s = 2)
Tytonidae (s = 1)
Aramidae (s = 1)
Trogonidae (s = 1)
0e+00
-1e-03
-2e-03
-3e-03
-4e-03
-5e-04
0e+00
5e-04
1e-03
Δr
Δl
c
Preferred habitat
Towns (s = 14)
Tundra (s = 5)
Forests (s = 143)
Oceans (s = 16)
Grasslands (s = 53)
Shorelines (s = 31)
Scrub (s = 60)
Rivers and Streams (s = 6)
Lakes and Ponds (s = 43)
Marshes (s = 61)
Open Woodlands (s = 94)
Deserts (s = 10)
0.0e+00
-5.0e-04
-1.0e-03
-1.5e-03
-2e-04
-1e-04
0e+00
1e-04
2e-04
Δr
Δl
d
Species
↑253
↓255
150
87
37
10
8
83
2
31
2
21
1
34
1
35
2
4
2000
10
0
−10
−2000
−4000
ΔN
Family
↑23
↓48
10
5
13
2
10
6
4
5
15
1
1000
10
0
−10
−5000
−10000
ΔN

Appendix A

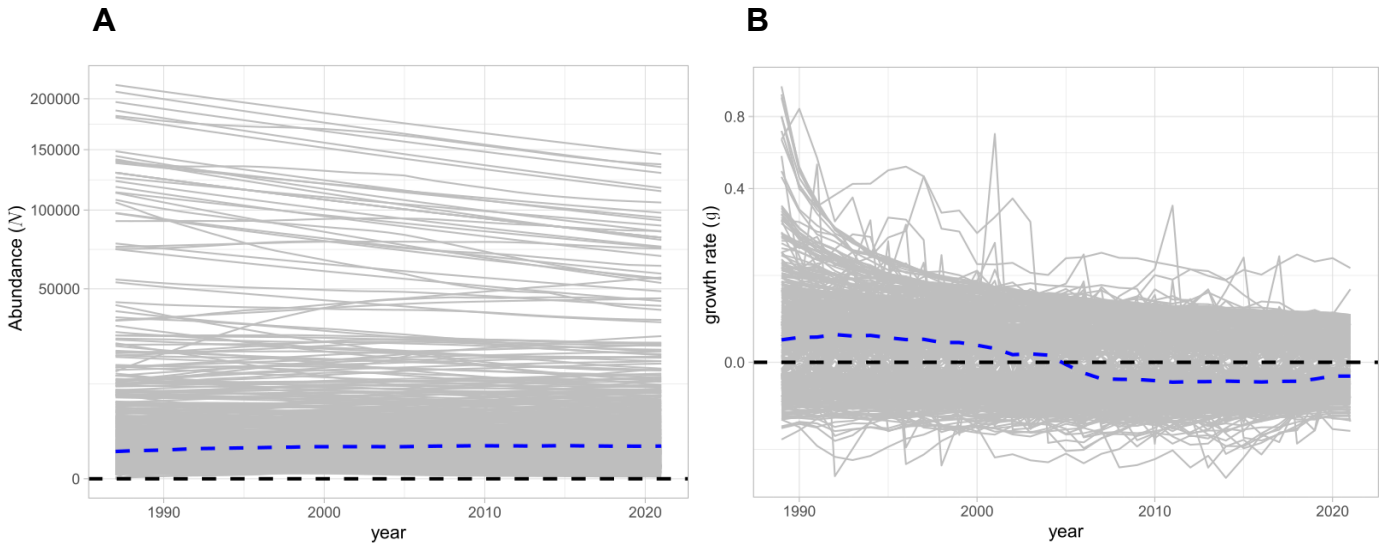

Appendix A Fig. 1: *Temporal change of* ***(A)*** *abundance (N) and* ***(B)*** *yearly growth rate (g) across North America. Each grey line represents the time-series for one of 508 species. The blue dashed line represents the median values for each year. The y-axis is on a square root scale.*

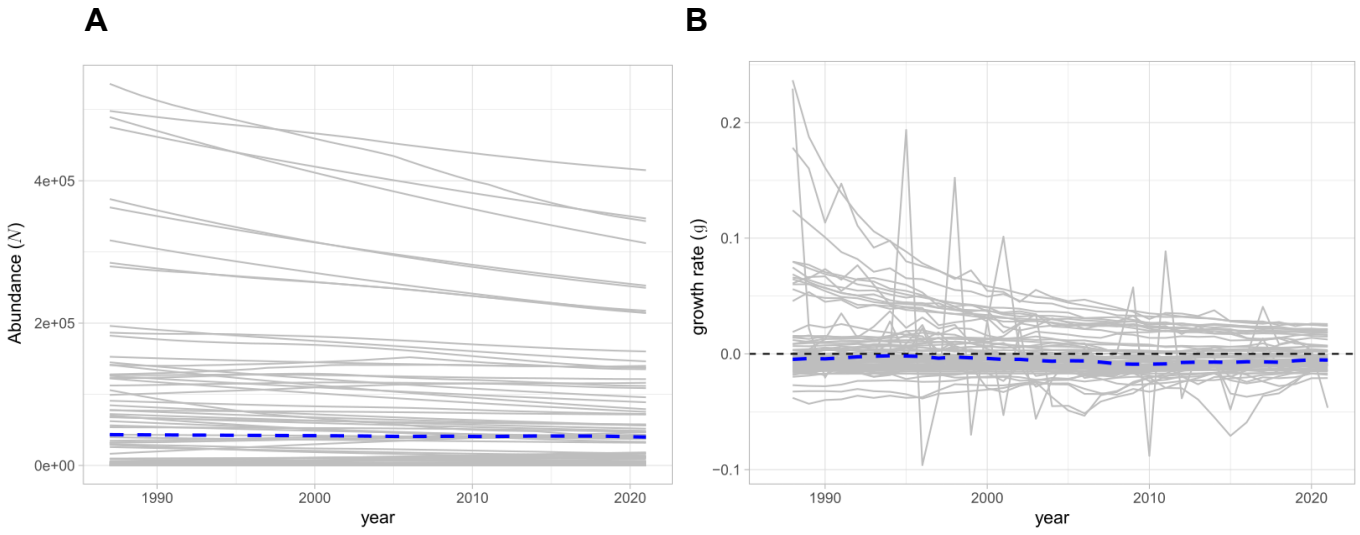

Appendix A Fig. 2: *Temporal change of* ***(A)*** *abundance (N) and* ***(B)*** *yearly growth rate (g) across North America. Each grey line represents the time-series for one of 71 bird families. The blue dashed line represents the median values for each year. The y-axis is not transformed in* ***(A)****, and log transformed (base 10) in* ***(B)****.*

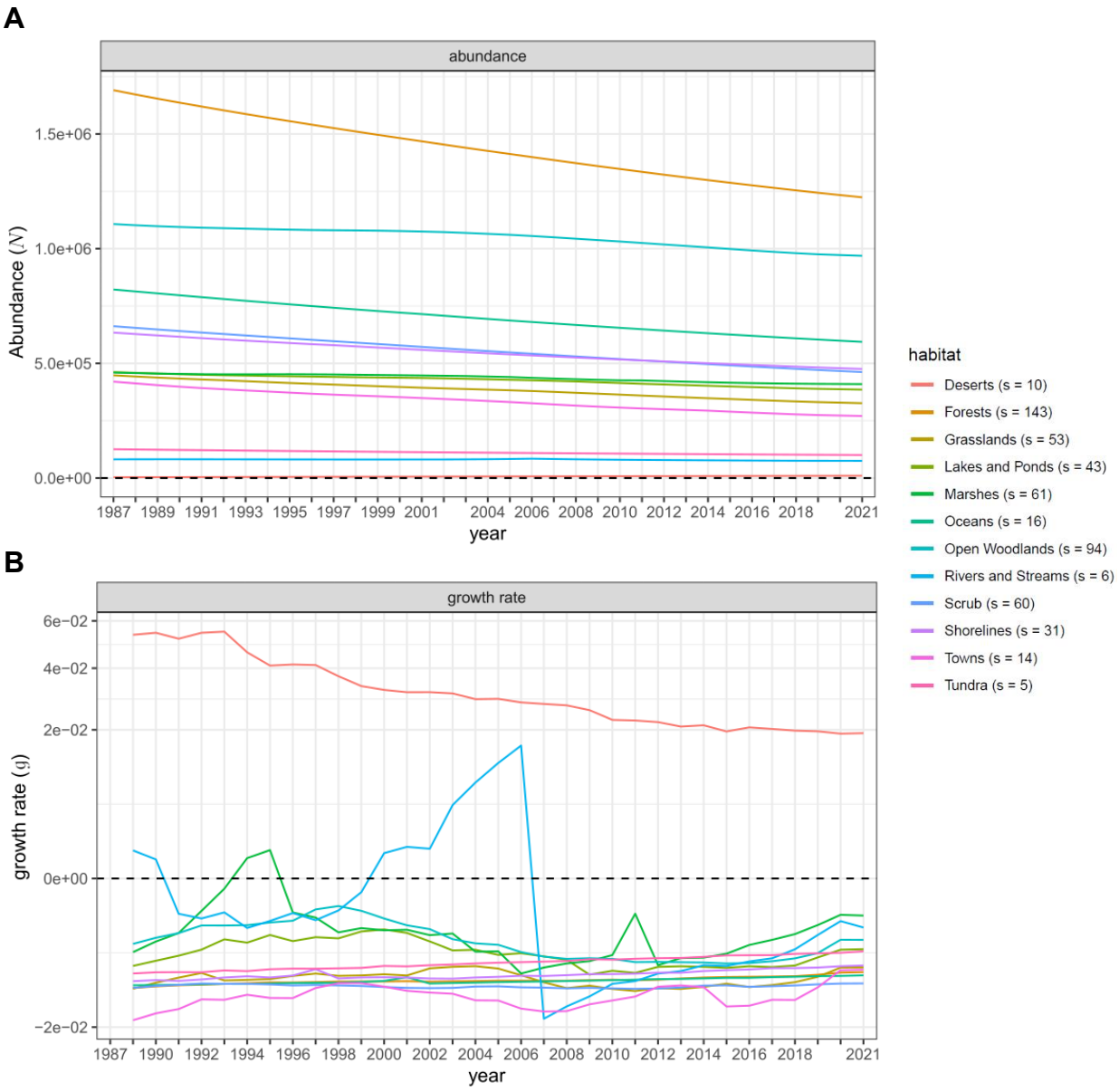

Appendix A Fig. 3: *Temporal change of* ***(A)*** *abundance (N) and* ***(B)*** *yearly growth rate (g) for each preferred habitat. The y-axis is not transformed in* ***(A)****, and square root transformed in* ***(B)****. The number of species for each preferred habitat is indicated by "s = number of species".*

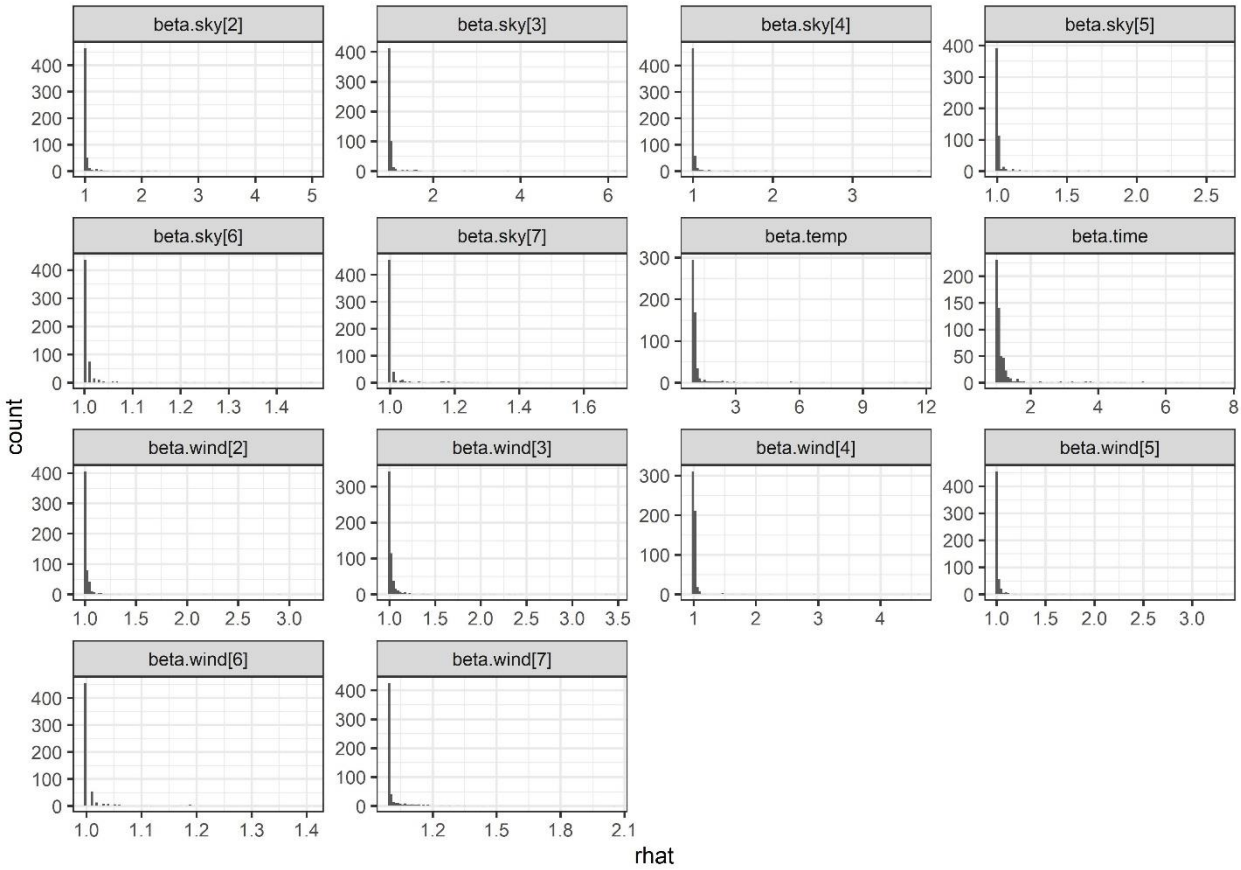

Appendix A Fig. 4: *Distributions of the $\hat{R}$ (rhat) values for 14 parameters and for 564 species. $\hat{R}$ compares the variance of parameter values between Markov Chain Monte Carlo (MCMC) chains to the variance of parameter values within chains. Values near 1 indicate likely convergence. We discarded species with $\hat{R} > 3$ for at least 1 parameter, ending up with 508 species that we report in the results.*